INTERNATIONAL ATOMIC ENERGY AGENCY
UNITED NATIONS EDUCATIONAL, SCIENTIFIC AND CULTURAL ORGANIZATION

INTERNATIONAL CENTRE FOR THEORETICAL PHYSICS
34100 TRIESTE (ITALY) - P.O.B. 586 - MIRAMARE - STRADA COSTIERA 11 - TELEPHONES: 224281/2/3/4/5/6
CABLE: CENTRATOM - TELEX 460392-1

SMR/100 - 2

WINTER COLLEGE ON LASERS, ATOMIC AND MOLECULAR PHYSICS

(24 January - 25 March 1983)

Atoms in very strong fields

D. KLEPPNER

Research Laboratory of Electronics
Massachusetts Institute of Technology
Cambridge, MA 02139
U.S.A.

Contents

R. Balian and J. C. Adam, eds.
Les Houches, Session XXXIV, 1980 – Interaction Laser–Plasma/Laser–Plasma Interaction

1. Introduction

In the past few years interest has grown in the structure of atoms in very strong fields stimulated by experimental studies with intense lasers and with highly excited atoms. There are two streams to this research; presently they follow separate paths, although we can hope that they will eventually merge. The first is the study of the dynamical effects of strong laser light on matter in which non-linear phenomena such as multi-photon ionization and photodissociation occur readily. Such non-linear processes can play significant roles in laser plasma interactions. The second stream, the subject of these lectures, is the study of the structure of atoms in strong static or quasi-static fields. For the most part, interest in this problem is essentially a matter of scientific curiosity. As we shall see, even the most elementary atomic system can display unexpected and sometimes dramatic phenomena in the presence of strong fields. The subject is attractive because the theoretical problem is simple to pose – and in some cases simple to solve – and because relatively elegant experimental pictures can be obtained. In principle a clear understanding of atoms in strong static fields is needed to understand their behavior in intense radiation fields. Someday we may have a single theory which covers the whole range of phenomena. For the present, we must be satisfied with a more restricted approach.

These lectures draw their examples chiefly from research carried out at Massachusetts Institute of Technology. This hardly does justice to the considerable body of research underway elsewhere, but the lectures are intended to be tutorial rather than serve as any sort of systematic review.

The presentation is divided into three sections. The structure of atoms in strong electric fields is discussed in section 2, and in section 3 the dynamics of field ionization is treated. Section 4 deals with the structure of atoms in strong magnetic fields.

2. The structure of atoms in strong electric fields

The study of atom–field interactions has been revolutionized by the use of highly excited atoms. As we shall see, by working with these atoms the relative strength of the atomic field and the applied field can be varied at will, opening many new avenues of research. As a starting point, let us consider the familiar Stark effect.

2.1. Background: the second order Stark effect

The interaction of an atom with a uniform electric field F along the z-axis is governed by the Hamiltonian

$$H_F = eF\sum_j z_j. \tag{2.1}$$

With the notable exception of hydrogen, atomic states of opposite parity are normally non-degenerate. Since the operator in eq. (2.1) is odd, its diagonal matrix elements vanish and we must invoke second order perturbation theory. The energy shift of level a is

$$\Delta E_a = e^2F^2\sum_b{}' \frac{|z_{ab}|^2}{E_a - E_b}, \tag{2.2}$$

where $z = \sum_j z_j$, the index j ranging over all electrons. Our chief interest is in atoms for which the contribution of a single electron dominates the matrix element and we shall regard z as a single electron operator. As is easily shown, z only connects states a and b for which $J_b = J_a, J_a \pm 1$ and $m_b = m_a$ where J is the total angular momentum and m is the eigenvalue of J_z. Physically, the second order Stark shift results from the polarization of the atom by the electric field. It is natural to write

$$\Delta E_a = -\tfrac{1}{2}\alpha_a F^2, \tag{2.3}$$

where α_a is the static polarizability of the atom. For calculational purposes the polarizability is most conveniently written as a second rank tensor [1], but for purposes here we can take

$$\alpha_a = \frac{2}{3}e^2\sum_b{}' \frac{|r_{ab}|^2}{E_b - E_a}. \tag{2.4}$$

Polarizability has the dimensions of volume; for the ground state of a single electron atom α is roughly the volume of the atom. The polarizability of the ground state of hydrogen, for example, is $4.5a_0^3$, where a_0 is the Bohr radius. [The "volume" of the atom is $(4\pi/3)a_0^3 = 4.2a_0^3$.] Polarizabilities of this magnitude are small in the sense that the Stark shift in a laboratory field is small compared to the energy difference between optical terms. If we take $\alpha = 100a_0^3$ and $F = 100$ kV/cm, we obtain, in spectroscopic units of cm^{-1}, $\Delta E = -4 \times 10^{-3}$ cm^{-1}. By way of comparison, a typical optical transition is 2×10^4 cm^{-1} and its Doppler width is 0.2 cm^{-1}. The Stark shift would be unobservable.

Opportunities for studying the Stark effect under controlled laboratory conditions are not as dismal as this estimate suggests, however, for the upper as well as the lower state contributes to the shift. The polarizability of an excited state is generally larger than that of the ground state, particularly if there is a nearby level of opposite parity. For instance, singly ionized argon has a 3d level with a polarizability of $-3 \times 10^4 a_0^3$ due to a 4p level which lies only 13 cm^{-1} below it. The Stark shift in a 100 kV/cm field is [2] 1.2 cm^{-1}, which is easily observed. Nevertheless, it is still small.

The fundamental reason that optical Stark shifts are small is that the static electric field we can apply will be small by atomic standards. A field of 10^6 V/cm is large by conventional laboratory standards but is feeble compared to the atomic unit of electric field, $e/a_0^2 = 5.14 \times 10^9$ V/cm. It is hardly surprising that small fields have small effects. Optical Stark shifts can teach us about matrix elements and polarizability, but if our aim is to seriously upset the atom, to fundamentally alter its structure in order to understand atomic behavior in intense fields, we will have to look elsewhere.

2.2. Stark shifts in Rydberg states

Our equations will take the simplest form if we use atomic units. In this system $e = \hbar = m_e = 1$; the unit of distance is the Bohr radius $a_0 = 5.29 \times 10^{-9}$ cm, the unit of energy is $e^2/a_0 = 27$ eV. (In terms of cm^{-1}, the atomic unit of energy is $2R = 2.19 \times 10^5$ cm^{-1}; R is the Rydberg constant.) Since $e^2/\hbar c = \alpha = (137)^{-1}$, $c = \alpha^{-1} = 137$. In these units the non-relativistic energy of hydrogen is

$$E_n = -\frac{1}{2n^2} \tag{2.5}$$

where n is the principle quantum number. The "good" quantum numbers are n, the angular momentum ℓ and the z component of angular momentum m. ℓ takes the values $0, \ldots, n-1$, and m takes the value $-\ell, \ldots, +\ell$. In non-relativistic hydrogen, all states of a given n are degenerate. In alkalis the ℓ-degeneracy is broken and the energy can be written

$$E_n(\ell) = -\frac{1}{2}\frac{1}{(n - \delta_\ell)^2}, \tag{2.6}$$

where δ_ℓ is the quantum defect, a constant or a very slowly varying function of n. The quantum defect is generally much less than one if ℓ is greater than two or three, depending on the particular alkali.

The energy splitting due to the quantum defect can play an important role in the behavior of atoms in strong fields. For highly excited states the energy separation between the states (n, ℓ) and (n, ℓ') is approximately

$$\Delta E_n \simeq \frac{\delta}{n^3} \tag{2.7}$$

where $\delta = \delta_\ell - \delta_{\ell'}$. Such states have an anomalous polarizability for the following reason: the radial matrix element between states of hydrogen (n, ℓ) and $(n, \ell' = \ell \pm 1)$ is roughly n^2. (The mean radius of the Bohr atom is approximately n^2, and we can expect the matrix element to scale as n^2 purely on dimensional grounds.) From eq. (2.4) we obtain

$$\alpha_a \sim \frac{|r|^2}{\Delta E} \sim n^7/\delta. \tag{2.8}$$

The n^7 dependence of the polarizability means that the second order Stark effect ΔE_a can become gigantic [3]. In particular, if we ask what field is required for ΔE_a to equal the separation between levels, we have $(1/2)\alpha_a F^2 = \Delta E_n$, or

$$F \sim \delta n^{-5}; \tag{2.9}$$

F diminishes very rapidly with n. For $\delta = 0.1$ and $n = 30$, $F = 20$ V/cm. Although 20 V/cm would not normally be regarded as large, for these atoms it produces a Stark shift as big as the term separation, which means that second order perturbation theory is inadequate. The atom is not merely perturbed, it is grossly distorted. We can expect many of its familiar properties to be radically altered.

According to eq. (2.8) the polarizability varies universely with δ. For hydrogen $\delta = 0$ and the polarizability diverges. The Stark effect becomes first order, and even a small electric field is very large in the sense that it can totally distort the atom from the "shape" with which we are familiar.

2.3. *The Stark structure of hydrogen*

The Stark effect in hydrogen is often used as a textbook's illustration of degenerate perturbation theory. For $n = 2$, for example the matrix element of z connects the states $a = (2, 0, 0)$ and $b = (2, 1, 0)$ where the states are designated by (n, ℓ, m). It is easily shown that $z_{ab} = 3$ (atomic units) and the first order energies are

$$\Delta E_2 = \pm 3F. \tag{2.10}$$

(Relativistic effects and the Lamb shift play important roles at very low fields, but we shall neglect them.) The eigenstates are

$$\psi_\pm = \frac{1}{\sqrt{2}}[(2,0,0) \pm (2,1,0)]. \tag{2.11}$$

These states have mixed parity and they display electric dipole moments. The dipole moments give rise to the linear Stark effect.

When we attempt to apply degenerate perturbation theory to higher levels of hydrogen we find that the problem becomes awkward. The number of degenerate levels in each term increases as n^2 and one is forced to solve ever larger secular equations. More seriously, off diagonal matrix elements between the different terms plays increasingly larger roles and one must include higher order perturbations. Fortunately, the potential $V = -Z/r + Fz$ leads to a Hamiltonian which is separable in parabolic coordinates and a complete solution is possible.

2.3.1. *Solution in spherical and parabolic coordinates*

The solution for hydrogen in parabolic coordinates bears some similarities to the familiar solution in spherical coordinates. Both problems are treated in the standard texts [4], but we shall need to refer to the results later and it will be helpful to have them on hand.

In the absence of an applied field Schrödinger's equation for hydrogen is

$$\Delta u + 2\left(E + \frac{Z}{r}\right)u = 0. \tag{2.12}$$

Taking $u = Y(\theta, \phi)R(r)$, we obtain the familiar angular solution

$$Y(\theta, \phi) = Y_{\ell, m}(\theta, \phi), \tag{2.13}$$

where $Y_{\ell, m}(\theta, \phi)$ is a spherical harmonic. The radial equation becomes

$$R'' + \frac{2}{r}R' + 2\left[E + \frac{Z}{r} - \frac{\ell(\ell+1)}{2r^2}\right]R = 0. \tag{2.14}$$

As $r \to \infty$, $R \sim \exp \pm\sqrt{(-2Er)}$. Letting $\varepsilon = \sqrt{(-2E)}$, and introducing the reduced coordinate $\rho = 2\varepsilon r$, we write $R(\rho) = \exp(-\rho/2)f(\rho)$, where $f(\rho)$ satisfies

$$f'' + \left(\frac{2}{\rho} - 1\right)f' + \left[\left(\frac{Z}{\varepsilon} - 1\right)\frac{1}{\rho} - \frac{\ell(\ell+1)}{\rho^2}\right]f = 0. \tag{2.15}$$

If we assume a power series solution in the form $f(\rho) = \rho^s L(\rho)$, where $L(\rho)$ is a polynomial, we find that for proper behavior as $\rho \to 0$, $s = \ell$.

$L(\rho)$ satisfies

$$\rho L'' + [2(\ell+1) - \rho]L' + [Z/\varepsilon - \ell - 1]L = 0. \tag{2.16}$$

If we write $L(\rho) = \sum_j a_j \rho^j$, then the recursion relation is:

$$a_{j+1} = 2\frac{j + \ell + 1 - Z/\varepsilon}{(j+1)(j+2\ell+2)} a_j. \tag{2.17}$$

For convergence the series must terminate which requires that Z/ε be an integer, n. This gives the Bohr relation

$$E = -\frac{Z^2}{2n^2}. \tag{2.18}$$

The function $L(\rho)$ is a Laguerre polynomial $L_{n+\ell}^{2\ell+1}(\rho)$. The number of radial nodes is the order of the polynomial: $n + \ell - (2\ell + 1) = n - \ell - 1$.

The long-range nature of the Coulomb potential gives the hydrogenic functions a number of distinctive properties including an infinite number of bound states and a very rapid increase of radius with n. It can be shown [4] that the mean radius for state (n, ℓ, m) is

$$\langle r \rangle = \frac{1}{2Z}[3n^2 - \ell(\ell+1)]. \tag{2.19}$$

For large n, $\langle r \rangle$ ranges between $(3/2Z)n^2$ and $(1/Z)n^2$ as the angular momentum ranges from zero to its maximum value.

We turn now to the solution in parabolic coordinates. These coordinates are defined by

$$\xi = r + z, \qquad \eta = r - z, \qquad \phi = \arctan(y/x). \tag{2.20}$$

Schrödinger's equation in zero field takes the form

$$\frac{4}{\xi+\eta}\left(\frac{\partial}{\partial\xi}\left(\xi\frac{\partial}{\partial\xi}\right) + \frac{\partial}{\partial\eta}\left(\eta\frac{\partial}{\partial\eta}\right)\right)u + \frac{1}{\xi\eta}\frac{\partial^2}{\partial\phi^2}u + 2\left[E + \frac{Z}{\xi+\eta}\right]u = 0. \tag{2.21}$$

This can be separated by multiplying by $(\xi+\eta)/4$ and writing $u(\xi, \eta, \phi) = f_1(\xi)g_2(\eta)e^{im\phi}$. We obtain

$$\frac{d}{d\xi}\left(\xi\frac{df_1}{d\xi}\right) + \left(\frac{1}{2}E\xi + Z_1 - \frac{m^2}{4\xi}\right)f_1 = 0 \tag{2.22}$$

where Z_1 is the separation constant. The equation for g_2 is identical in form except that the separation constant is $Z_2 = Z - Z_1$.

Using the same arguments we employed in the solution of $R(r)$, we conclude that f_1 must behave like

$$f_1 = e^{-x/2}x^{|m|/2}F_1(x) \tag{2.23}$$

where $x = \sqrt{(-2E)}\,\xi = \varepsilon\xi$. $F_1(x)$ satisfies

$$xF_1'' + (|m| + 1 - x)F_1' + \left(\frac{Z_1}{\varepsilon} - \frac{|m|+1}{2}\right)F_1 = 0. \tag{2.24}$$

This is identical in form to eq. (2.16), and we have

$$F_1 = L_{n_1+|m|}^{|m|}(x) \tag{2.25}$$

where n_1 is a non-negative integer given by

$$n_1 = \frac{Z_1}{\varepsilon} - \frac{1}{2}(|m| + 1). \tag{2.26}$$

The corresponding solution for $g_2(\eta)$ yields

$$n_2 = \frac{Z_2}{\varepsilon} - \frac{1}{2}(|m| + 1). \tag{2.27}$$

Imposing the constraint $Z_1 + Z_2 = Z$ then gives

$$E = -\frac{Z^2}{2n^2} \tag{2.28}$$

as before, where the integer n is now given by

$$n_1 + n_2 + |m| + 1 = n. \tag{2.29}$$

The parabolic functions are the products of polynomials having n_1 nodes along the ξ-axis and n_2 nodes along the η-axis. The "center of charge" can be shown to be at

$$\langle z \rangle = \tfrac{1}{2}n(n_1 - n_2), \tag{2.30}$$

which means that the parabolic states have permanent dipole moments.

2.3.2. The "shape" of hydrogen

We have obtained exact analytic solutions for the states of hydrogen in both spherical and parabolic representations. The existence of such solutions means that many properties of the atom can be calculated exactly in closed form, but the solutions do not necessarily provide much insight into the structure of the atom. It is not easy to visualize the products of polynomials in three dimensions. Fortunately, the computer can be of assistance here. Figures 1 and 2 show the charge distribution in

the $n = 8$, $m = 0$ states of hydrogen in the spherical and parabolic representations, respectively. The plots represent the charge density $|\psi|^2$ in a "slice" through the atom along the z-axis. The charge density has been multiplied by r^2 to make the features more visible. The actual charge densities have azimuthal symmetry around the z-axis. The dipole moments and parabolic nodal lines are clearly visible in fig. 2.

2.3.3. Solution in an electric field

If an electric field term $+Fz = +F(\xi - \eta)/2$ is added to the Hamiltonian, eq. (2.22) becomes

$$\frac{\mathrm{d}}{\mathrm{d}\xi}\left(\xi\frac{\mathrm{d}f_1}{\mathrm{d}\xi}\right) + \left(\frac{1}{2}E\xi + Z_1 - \frac{m^2}{4\xi} - \frac{1}{4}F\xi^2\right)f_1 = 0. \tag{2.31}$$

The companion equation for η is

$$\frac{\mathrm{d}}{\mathrm{d}\eta}\left(n\frac{\mathrm{d}g_2}{\mathrm{d}\eta}\right) + \left(\frac{1}{2}E\eta + Z_2 - \frac{m^2}{4\eta} + \frac{1}{4}F\eta^2\right)g_2 = 0. \tag{2.32}$$

These equations can be solved exactly by perturbation theory in the sense that if we write

$$E = \sum_j E_j \tag{2.33}$$

where E_j is a term in a power series expansion in the field

$$E_j = a_j F^j, \tag{2.34}$$

then the coefficients $a_j(n, n_1, n_2, |m|)$ can be found exactly. The procedure is to treat eq. (2.32) as an eigenvalue equation for the separation constant. $Z_{1,2}(E, n_{1,2}, |m|, F)$ is found by perturbation theory to the desired order in the field, and then the coupling equation $Z_1 + Z_2 = Z$ is used to derive E as a function of F. Through second order the results are (taking $Z = 1$)

$$E_0 = -\frac{1}{2n^2}, \qquad E_1 = \frac{3}{2}n(n_1 - n_2)F, \tag{2.35a,b}$$

$$E_2 = -\frac{1}{16}n^4\left(17n^2 - 3(n_1 - n_2)^2 - 9m^2 + 19\right)F^2. \tag{2.35c}$$

Because the Stark interaction $+Fz$ is invariant under rotation about the z-axis, the degeneracy between states with azimuthal quantum numbers m and $-m$ remains in the presence of an electric field. Thus E_1 is independent of m, while E_2 depends on m^2.

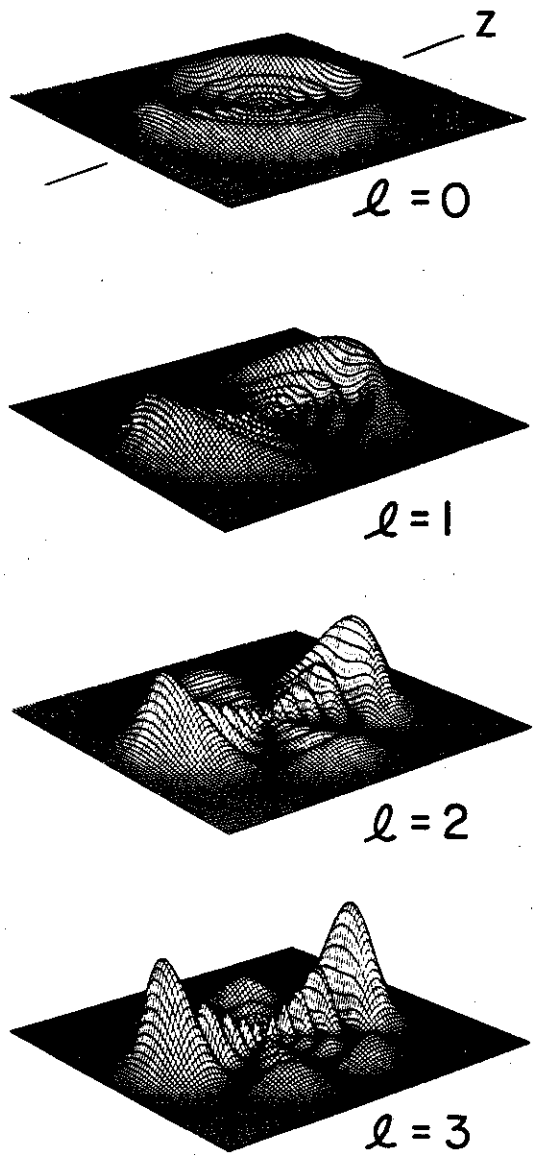

Fig. 1. The charge distribution for hydrogen in a plane containing the z-axis. The charge density has been multiplied by r^2 to aid visibility. The states are $n = 8$, $m = 0$, $\ell = 0$–7.

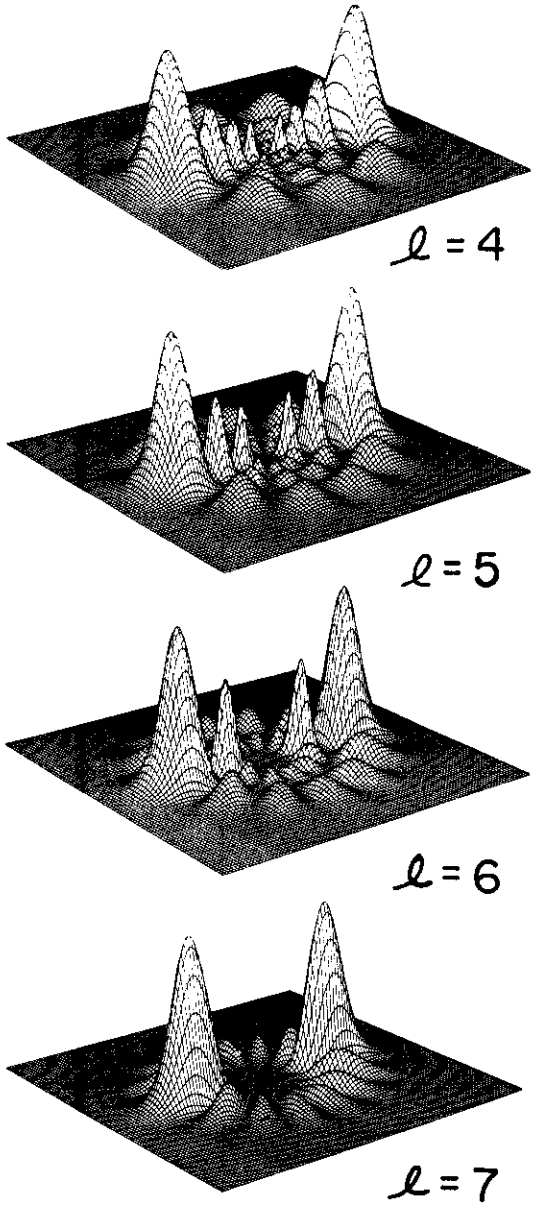

Fig. 1 continued.

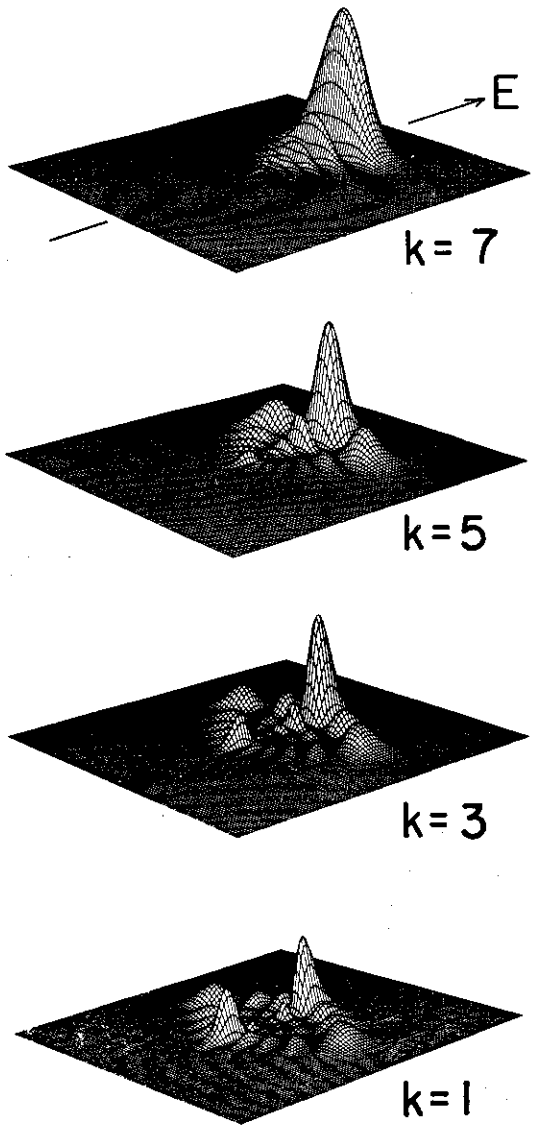

Fig. 2. The charge distribution for hydrogen, displayed as in fig. 1, for the "parabolic" representation. The states are $n = 8$, $m = 0$, $k = -7 \rightarrow 7$ ($k = n_1 - n_2$). The dipole moments which give rise to the first order Stark effect are conspicuous. Note that the nodal lines form families of parabolas.

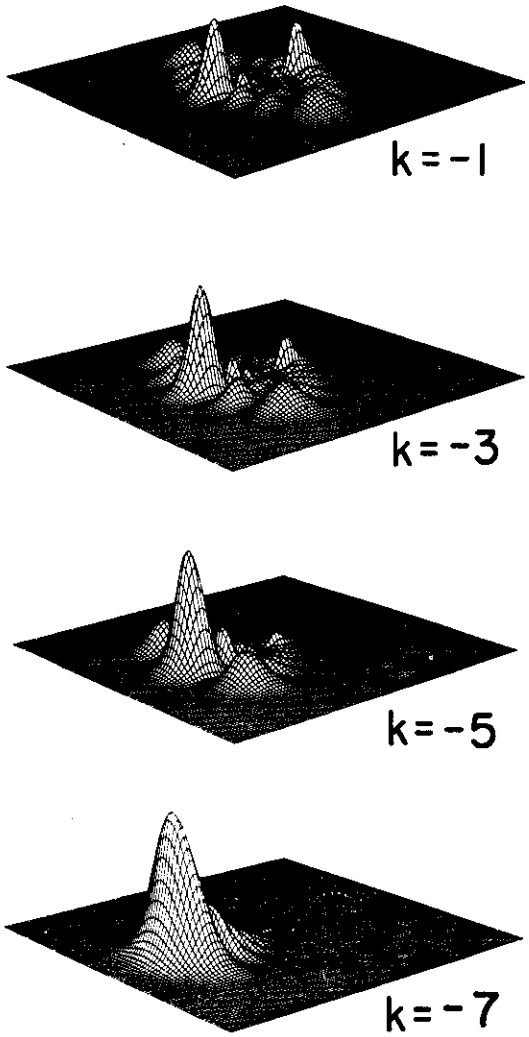

Fig. 2 continued.

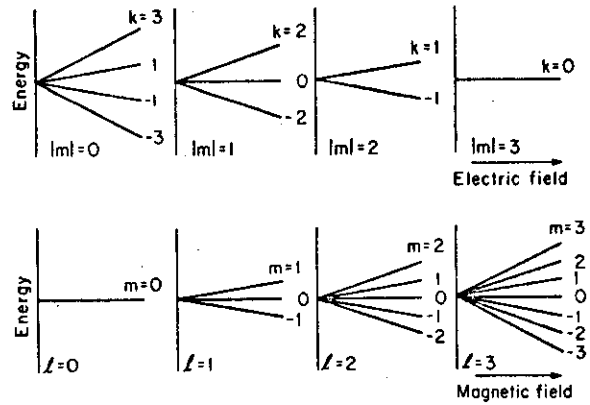

Fig. 3. Energy level for $n = 4$ states of hydrogen in an electric field (above) and a magnetic field (below).

To understand the major features of the Stark structure we must use a result which will be explained later: for a sufficiently large field, atoms start to ionize and the bound state solutions no longer apply. A characteristic size is $F_c = 1/(16n^4)$. If we compare the maximum value of E_1 and E_2 at F_c we find $|E_2/E_1| \simeq \frac{2}{3}(n^4F_c) \simeq 4\%$. Thus the first order energy dominates the level structure diagram. The Stark interaction separates every term n into a series of manifolds labeled by $|m| = 0, 1, \ldots, n-1$. Each manifold is split by E_1 into a series of sublevels whose energy can be written $E_1 = \frac{3}{2}nF(n_1 - n_2) = \frac{3}{2}nFk$, where the parabolic quantum numbers take the values $k = n - |m| - 1, n - |m| - 3, \ldots, -n + |m| + 1$. The levels for $n = 4$ are sketched in fig. 3. For comparison, we also show the states in a low magnetic field $\boldsymbol{B}$ where the Hamiltonian is, neglecting spin, $H_m = g_j\mu_0 \boldsymbol{L} \cdot \boldsymbol{B} = g_j\mu_0 Bm$. The Stark structure for $m = 0$ states of hydrogen in the range $n = 4$–6 is shown in fig. 4. An important feature, which we shall discuss further, is that the energy levels from different terms cross without any apparent repulsion.

2.3.4. High order contributions to the Stark effect

The procedure for calculating the energy can be carried out to higher order, but the calculations are so cumbersome that until recently E_4 was the highest term known. In an important advance, Silverstone [5] developed a general method for obtaining the perturbation coefficient to *any* order so that now as many terms as desired can be employed.

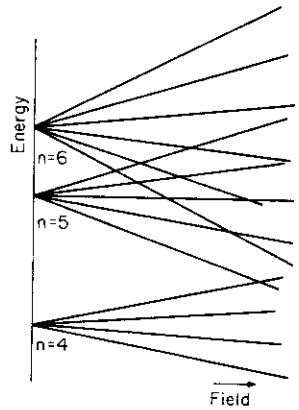

Fig. 4. Energy levels for hydrogen in an electric field in the region of $n = 4-6$, for $m = 0$ states. Note that the levels cross sharply.

In spite of having this general solution, several difficulties remain in our understanding of single electron atoms in strong electric fields. The first is that perturbative power series solutions are only asymptotically convergent. Thus as more terms are added in eq. (2.33), the solution eventually gets worse. This is rather dramatically demonstrated in a comparison of theory with a measurement of the Stark energy of several levels of hydrogen in an experiment by Koch [6], using precision laser spectroscopy. Figure 5 shows the theoretical result as an increasing number of terms are kept.

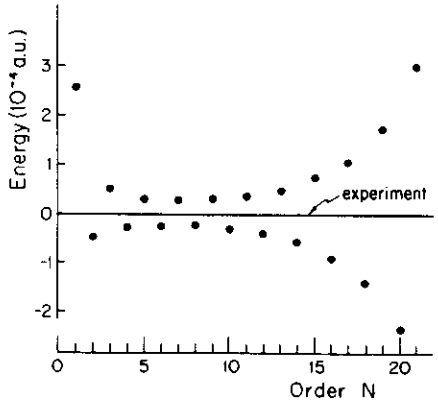

Fig. 5. Energy for hydrogen in an electric field as given by pertubation theory carried out to successively higher order (dots) compared to the experimental value (solid line). The state is $n = 25$, $k = 19$, $|m| = 1$, and the field is 2514(3) V/cm. (From Koch, ref. [6].)

Fortunately, various techniques are available for treating asymptotic series. Padé approximants are one such method, and these have been successfully applied to the hydrogen Stark problem by Silverstone and Koch [7].

A more troublesome problem is that at high fields, ionization processes become important. Stationary state solutions inherently fail and different approaches are needed. We shall return to this problem later.

Another problem is that our solution for hydrogen has neglected relativistic effects, electron spin and other perturbations. As we shall see, small perturbations sometimes have major consequences. For one-electron atoms other than hydrogen, these perturbations can play dominant roles. We turn now to the problem of the Stark structure of simple non-hydrogenic atoms.

2.4. Stark structure of the alkali-metal atoms

2.4.1. A digression on quantum defects

Rydberg's quantum defect formula, eq. (2.7), was discovered empirically, but the formula can be motivated by simple physical arguments. It is helpful to understand these, for we shall frequently use quantum defects to parameterize departures of the potential from the Coulomb potential.

For a single electron in a neutral atom moving around a core of closed shell electrons, the potential at large distances is $-1/r$. At short distances the potential is much stronger, dropping to $-Z/r$ near the nucleus. The potential departs from $-1/r$ rather abruptly as r approaches the radius of the core, typically a few atomic units. For highly excited states, however, the electron spends most of its time outside the core, and the core can be treated as a perturbation. It should be pointed out, however, that the perturbation does not vanish as the principle quantum number increases; its effect is constant and the electron's state *never* becomes hydrogenic.

We can make the argument quantitative by employing a WKB solution to the radial equation $R(r)$. If we let $U(r) = rR(r)$, Schrödinger's equation for hydrogen is, in atomic units,

$$U'' + 2\left(E + \frac{1}{r} - \frac{\ell(\ell+1)}{2r^2}\right)U = 0. \tag{2.36}$$

The eigenstates for $U(r)$ can be obtained from the phase integral

equation,

$$\int_a^b k_c \, dr = \left(p + \frac{1}{2} \right) \pi. \tag{2.37}$$

where p is an integer and

$$k_c = \left(2E + \frac{2}{r} - \frac{(\ell + \frac{1}{2})^2}{r^2} \right)^{1/2}. \tag{2.38}$$

The limits of the integral are the zeros of the integrand. In k_c we have made the semiclassical correspondence $\ell(\ell + \frac{1}{2}) \to (\ell + \frac{1}{2})^2$. Evaluation of the integral yields,

$$\left(k_c r - \frac{1}{\varepsilon} \sin^{-1}\left[2\frac{1 - \varepsilon^2 r}{\Delta} \right] - \frac{1}{\ell + \frac{1}{2}} \sin^{-1}\left(2\frac{1 - (\ell + \frac{1}{2})^2 / r}{\Delta} \right) \right)_a^b = (p + \tfrac{1}{2})\pi, \tag{2.39}$$

where $\varepsilon^2 = -2E$ and $\Delta = 2(1 + 2E(\ell + \frac{1}{2})^2)^{1/2}$. The result is $\pi/\varepsilon - (\ell + \frac{1}{2})\pi = (p + \frac{1}{2})\pi$ or $E = -(1/2n^2)$ where $n = p + \ell + 1$.

We can apply the argument to an alkali by modifying eq. (2.38). Since the potential is approximately $-1/r$ outside of the core, we have

$$k = \begin{cases} \left[2E + 2V(r) - (\ell + \frac{1}{2})^2 / r^2 \right]^{1/2}, & r < r_c, \\ k_c, & r > r_c. \end{cases} \tag{2.40}$$

Equation (2.37) becomes

$$\int_{a'}^b k \, dr = (p + \tfrac{1}{2})\pi, \tag{2.41}$$

where a' is the new inner turning point. This can be rewritten

$$\left(\int_{a'}^{r_c} k \, dr - \int_a^{r_c} k_c \, dr \right) + \int_a^b k_c \, dr = \left(p + \frac{1}{2} \right) \pi. \tag{2.42}$$

The integrals within the brackets are restricted to the core region where $|V(r)|$ and $|1/r|$ are both much greater than $|E|$. If we simply neglect E, the bracketed term is a constant phase, ϕ_ℓ. We have

$$\int_a^b k_c \, dr = \left(p - \frac{\phi_\ell}{\pi} + \frac{1}{2} \right) \pi \tag{2.43}$$

which is similar to eq. (2.37) and has the solution

$$E = -\frac{1}{2} \frac{1}{(n + \delta_\ell)^2} \tag{2.44}$$

where $\delta_\ell = \phi_\ell/\pi$. The quantum defect is a measure of the phase shift arising from the non-Coulombic potential. (It can be shown that ϕ_ℓ is also the scattering phase shift for a low energy electron incident on the ionic core.) The accuracy of the approximation obviously depends on the ratio of E to V near the core. $|E| \sim \frac{1}{2}n^2$, and $|V| > 1/r_c$, so that the ratio is less than $r_c/2n^2$. Since r_c is a few atomic units, the approximation is very good for large n. If higher accuracy is needed, it is a simple matter to expand the phase integral in this ratio. In this case the quantum defect becomes a slowly varying power series in the energy.

It is apparent that *any* short range perturbation of the Coulomb potential can be characterized by a set of quantum defects, which is why they make such a useful set of parameters for studying electronic structure in non-Coulombic fields. In general, the quantum defects are very small once the angular momentum is large enough for the centrifugal barrier to exclude classically the electron from the perturbed region. For the alkalis, the quantum defects are large for ℓ less than or equal to the maximum angular momentum of the core, and then rapidly drop with increasing ℓ. Some representative values are given in table 1.

The natural unit of energy for highly excited atoms is the separation between adjacent terms:

$$\Delta E_0 = \frac{1}{2n^2} - \frac{1}{2(n+1)^2} \simeq \frac{1}{n^3}. \tag{2.45}$$

In terms of this unit the displacement of a level from the hydrogenic value is

$$\Delta E(\delta) = \frac{1}{2(n - \delta)^2} - \frac{1}{2n^2} \simeq \frac{\delta}{n^3} = \delta \Delta E_0. \tag{2.46}$$

Table 1

Alkali	$\ell = 0$	1	2	3
Lithium	0.4	0.05	< 0.01	< 0.01
Sodium	1.35	0.85	0.014	< 0.01
Potassium	2.18	1.7	0.27	< 0.01
Rubidium	3.14	2.65	1.3	?
Cesium	4.1	3.6	2.5	0.03

2.4.2. Stark structure of the alkalis

The single electron Hamiltonian containing a central potential plus the Stark interaction $+Fz$ permits Schrödinger's equation to be separated only if the central potential is exactly $-1/r$. Although the vast body of theoretical effort on atoms in strong fields has been on the hydrogen atom, it turns out that the hydrogen problem is in many ways unique. As mentioned previously, the static and dynamical properties of a one-electron atom can be dramatically altered by a small departure from a pure Coulomb potential. The alkali metal atoms provide excellent theoretical and experimental testing grounds for studying these effects.

The structure of alkalis in strong fields must be analyzed by perturbation theory or some other approximation method. Numerical methods based on solving the secular equation have been employed with considerable success [8]. The natural basis set is the spherical (angular momentum) representation

$$\psi(n^*, \ell, m) = R(n^*, \ell) Y_\ell^m(\theta, \phi), \tag{2.47}$$

where $n^* = n - \delta_\ell$ is the effective quantum number and $Y_\ell^m(\theta, \phi)$ is a spherical harmonic. Radial matrix elements of the electric field operator $Fz = Fr\cos\theta$ can be calculated by power series methods or by numerical integration of the radial equation. The angular part gives the dipole selection rules $\Delta\ell = \pm 1$, $\Delta m = 0$. The matrix representing the Hamiltonian is diagonalized by computer to yield the eigenenergies at each desired field.

The results for one such computation are shown in fig. 6. The atom is lithium, and the $|m| = 1$ states are shown in the vicinity of $n = 15$. This is a particularly simple case because only the p state has a significant quantum defect, $\delta_1 = 0.05$. For $\ell > 1$ the quantum defects are, for purposes here, negligible. The effect of δ_1 is visible at zero field; the $15p$ state is noticeably depressed below the degenerate manifold of states $n = 15, |m| = 1, \ell = 2, \ldots, 14$. At low electric fields the p state displays a second order Stark shift while the degenerate manifold shows a first order splitting. Above 500 V/cm the Stark interaction is so large that the p state has a first order Stark effect and the diagram appears to be hydrogenic.

The $m = 0$ states provide an interesting contrast to the $|m| = 1$ states. The s-state quantum defect is 0.4, which means that the s levels lie almost midway between the manifolds of adjacent terms $(n, m = 0, \ell = 1, 2, \ldots)$. Because the s levels are repelled almost equally by the p states above and below, they display extremely weak second order Stark effect

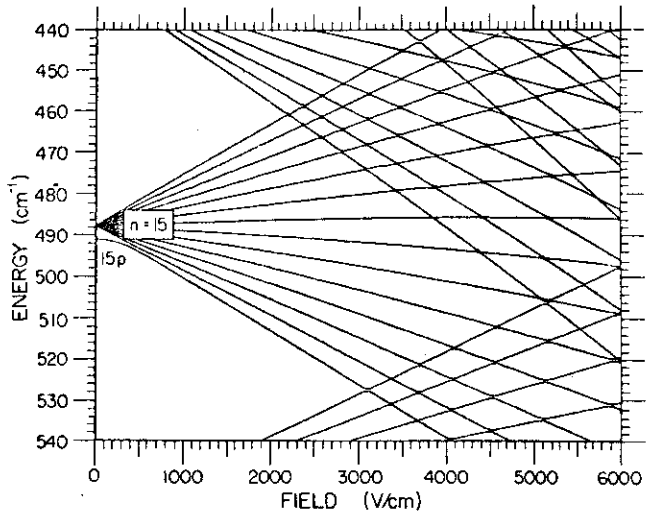

Fig. 6. Stark structure of lithium, $|m| = 1$, in the vicinity of $n = 15$. (From ref. [8].)

at low fields. As fig. 7 shows, however, the s states dramatically alter the Stark structure of all the states. All the Stark levels repel strongly and at high fields the slopes of the levels, which are proportional to the effective dipole moment, bear essentially no relation to the low field slopes. Occasional degeneracies (apparent level crossings) appear to occur with no particular order.

It is striking that a single quantum defect can so radically alter the Stark structure of an atom. The physical explanation lies in the fact that if one regards the hydrogenic Stark states as a linear superposition of spherical states, then a great deal of cancellation of wavefunctions occurs to produce the dipole charge distributions that are shown in fig. 2. Removing a single spherical state from the manifold upsets the delicate balance, and causes a major redistribution of charge.

The Stark structure of the heavier alkalis can be even more complex, particularly when fine structure is important enough to be included. Nevertheless, it can be understood in detail by following the approach we have used for lithium [8].

2.4.3. Experimental observation of the Stark structure of the alkalis

The Stark structures of the alkali Rydberg states have been studied experimentally with a combination of atomic beam and tunable laser techniques. By using atomic beams, the atoms can be observed in

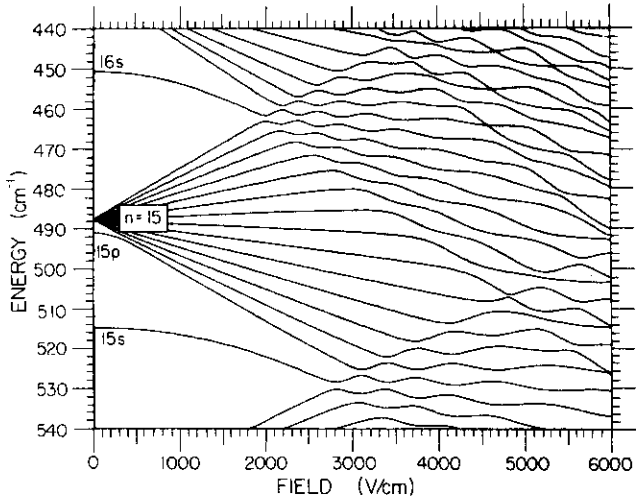

Fig. 7. Stark structure of lithium, $m = 0$, in the vicinity of $n = 15$. The large quantum defect of the s state radically alters the level structure (cf. fig. 6). (From ref. [8].)

isolation or in well controlled applied fields. The tunable lasers allow the atom to be prepared in well resolved states. Figure 8 shows a typical experimental setup. The atomic beam and laser beams intersect in a small interaction volume. Generally two or three optical photons are needed to excite an atom to a high-n level. In lithium, for instance, three lasers are used. The lasers are pulsed; 5 ns pulse length is typical. If the lasers are all on resonance thousands of atoms are left in a Rydberg state at the end of the pulse. Rydberg states are relatively long lived against spontaneous radiative decay, typically several microseconds or longer, and for many purposes they can be regarded as stable. The atom can be most easily detected with a strong electric field which ionizes them by a process we shall discuss in the next lecture. The ionizing field is provided by a high voltage pulse applied to two field plates on either side of the interaction region. The ionizing pulse is applied roughly 1–3 μs following the laser pulses. The emitted electrons or ions pass through a grid in the field plate and are detected by an electron multiplier or other charge-sensitive device. For studying the Stark structure, a DC electric field is applied to the field plates. A record of the integrated ionization current is stored by computer as the laser is swept across the energy region of interest. The process is repeated at successively higher electric fields. The spectra can then be displayed in an array with each plot located at its

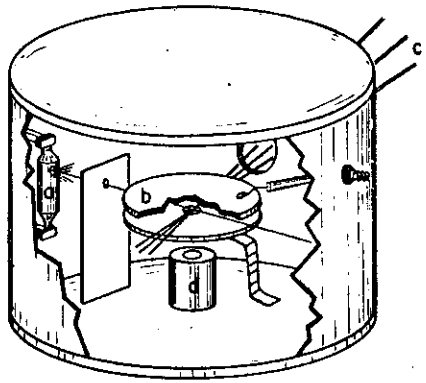

Fig. 8. Experimental setup for observing Stark structure of Rydberg atoms: A, atomic beam source; B, electric field plates; C, pulsed laser beams; D, electron multiplier.

electric field value. The result is an experimental map of the energy levels in an applied field. An example is shown in fig. 9. (The energy levels are most conspicuous when viewed with the eye close to the plane of the paper to the right or the left.) For quantitative study, the theoretical and experimental plots are superposed; the agreement is within the laser resolution.

Experimental Stark plots for the $m = 0$ states of lithium are shown in fig. 10. The intensity variations are due to variations in the oscillator

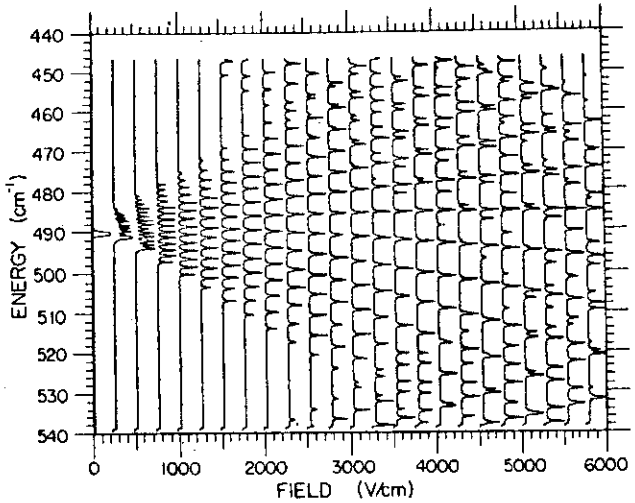

Fig. 9. Experimental map of the Stark structure of lithium, $|m| = 1$ (cf. fig. 6). (From ref. [8].)

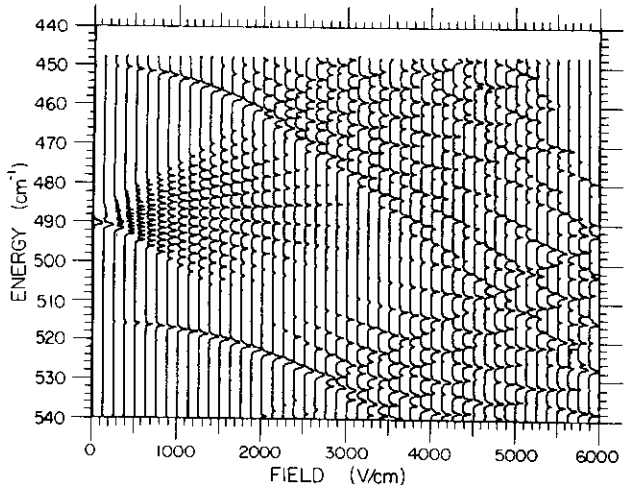

Fig. 10. Experimental map of the Stark structure of lithium, $|m| = 0$. The variations in oscillator strength are not shown in the theoretical plot (fig. 7), but they are in good agreement with the calculated values. (From ref. [8].)

strength. The laser excites the transition $3s-np$, and the intensity of the excitation signal depends on the amount of p-state in each Stark level. Calculating the eigenvectors and eigenvalues for the Stark states are similar problems, and both agree with the experiment within the experimental resolution.

2.4.4. Level anti-crossings

Because Stark levels cross for the non-relativistic case in hydrogen, the size of the anti-crossings provides a sensitive test of our understanding of the Stark structure of quasi-hydrogenic atoms. Interaction between levels are smallest for states which have little overlap, which means states with opposite Stark slopes. They are also smallest for systems with small quantum defects. Figure 11 shows the calculated and measured level separation for the uppermost member of the $n = 18, |m| = 1$ manifold of lithium, and the second lowest member of the $n = 19, |m| = 1$ manifold. The largest quantum defect is $\delta_l = 0.05$ (a cw laser was used here to improve the experimental resolution). Theory and experiment agree to within 0.01 cm^{-1}, which is the estimated limit of numerical accuracy. An interesting feature is the disappearance of one level at the anticrossing. This is because the eigenstates at the anti-crossings are symmetric and antisymmetric combinations of the two unperturbed states. (The perturbation is the core potential.) The matrix elements between the $3s$ and

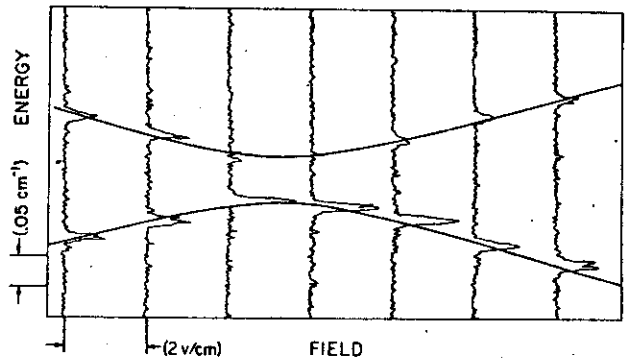

Fig. 11. An experimental plot of a level anti-crossing in lithium. The levels are $n = 18$, $k = 16$, $|m| = 1$ and $n = 19$, $k = -15$, $|m| = 1$. The solid lines are the calculated energy levels. Disappearance of one level at the anti-crossing is due to destructive interference between the matrix elements. In the other level the interference is constructive and the intensity is augmented. (From ref. [8].)

these Rydberg states add for one level and subtract for the other, with the result that the oscillator strength is transferred almost entirely to a single level.

2.4.5. Summary

We have shown that the Stark structure of one-electron atoms can be found from knowledge of the zero-field energies. If one or more of the quantum defects is large, typically large compared to 0.05, the Stark structure bears little resemblance to that of hydrogen. Nevertheless, we can calculate the structure reliably, an important step toward understanding the dynamical properties. Measurements of the structure give us confidence that the calculations are realistic. The ability to observe individual levels permits us to study further properties of atoms in strong electric fields with a clear understanding of just what states we are examining.

3. Ionization processes in a static electric field

3.1. Classical considerations

Classical arguments based on energy consideration can provide some useful insights into field ionization. As our starting point we will consider an overly simplistic classical model which turns out to be very helpful; in

many applications the model gives more useful results than elaborate quantum mechanical treatments!

The potential for a single electron in a Coulomb field and an applied field F along the negative z-axis is

$$V_F(r) = -\frac{1}{r} + Fz. \tag{3.1}$$

V_F has a maximum on the z-axis at $z = -1\sqrt{F}$. This maximum is actually a saddlepoint since V increases off the z-axis. The saddlepoint potential is

$$V_{sp} = -2\sqrt{F}. \tag{3.2}$$

For a state to be bound, its energy must be below the V_{sp}, or

$$E < -2\sqrt{F}. \tag{3.3}$$

According to this picture, if the electric field applied to a Rydberg atom is slowly increased, the atom will ionize at a critical value

$$F_c = \frac{E^2}{4}. \tag{3.4}$$

For a crude estimate of the critical field, we can neglect the Stark effect and take $E = -1/(2n^2)$. This yields

$$F_c^* = \frac{1}{16n^4}, \tag{3.5}$$

In laboratory units, $F_c^* = 3.2 \times 10^8/n^4$ V/cm: for $n = 30$, $F_c^* = 400$ V/cm. In many cases, ionization actually occurs at a field close to F_c^*. For instance, if a Rydberg state is populated and an electric field pulse is then applied, the atoms often start to ionize abruptly when the pulse amplitude reaches a field close to F_c^*. An example of this threshold behavior is shown in fig. 12, and a plot of the measured threshold field for a number of s-states in sodium is shown in fig. 13. For an alkali in an s-state we might expect to replace the principal quantum number by the effective principal quantum number $n^* = n - \delta_0$, so that eq. (3.5) becomes $F_c^* = 1/(16n^{*4})$. The data show the predicted $1/n^{*4}$ dependence. The displacement between the experimental and theoretical plots is not surprising in view of the fact that we have neglected the shift in energy due to the Stark effect.

The data in fig. 13 show that, in this case at least, field ionization obeys a simple well-defined scaling law. In fact, the threshold field is so well-defined that by measuring it one can often determine the state of the atom. The ability to analyze an atom's state from its ionization properties

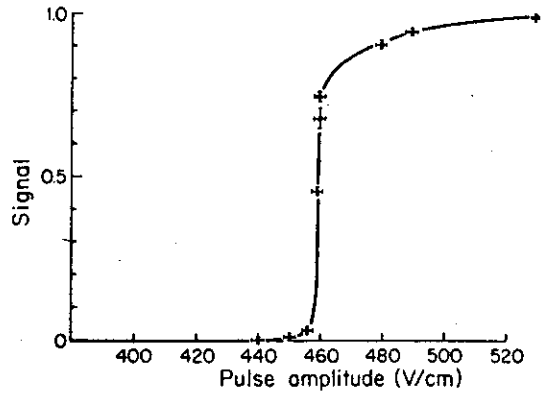

Fig. 12. Ionization signal vs. amplitude of electric field for pulsed ionization of the 3s state of sodium.

has made field ionization an extremely important tool in the study of Rydberg atoms.

Field ionization has a number of other features which make it experimentally attractive for detecting Rydberg atoms. It is extremely efficient; above the critical field essentially every Rydberg atom is ionized, and the electron or ion can be detected with an electron multiplier or other charge sensitive device with close to 100% efficiency. Field ionization is highly selective; atoms in low-lying states have effectively zero probability of being ionized. Thus a very small number of Ryberg atoms can be detected in the presence of a large background population. Experiments

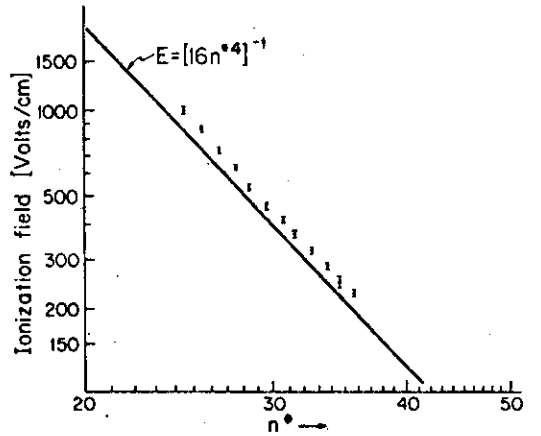

Fig. 13. Threshold field vs. effective quantum number for a sequence of sodium s states.

in which single atoms are detected are not uncommon. Finally, field ionization detectors are relatively inexpensive and simple to construct.

In deriving the criterion for stability we neglected the atom's angular momentum. We can, however, include angular momentum into our classical model by a simple argument [9]. Although total angular momentum is not a constant of motion due to the non-central field $\boldsymbol{F}$, J_z, the component of angular momentum about the z axis, is conserved. Denoting the magnitude of J_z by m, we have an effective potential

$$V_{\text{eff}} = -\frac{1}{r} + Fz + \frac{m^2}{2\rho^2}, \tag{3.6}$$

where $\rho^2 = x^2 + y^2$. The effect of the last term, the centrifugal potential, is to displace the saddlepoint from the z-axis and to raise it. The result is a slight correction to eq. (3.3), which becomes

$$E < -2\sqrt{F} + |\, m \,| F^{3/4} + \tfrac{3}{16} m^2 F. \tag{3.7}$$

For low $|\, m \,|$ states, the last two terms represent a small correction which shifts the threshold field by a few percent at most.

These ideas have been demonstrated experimentally by panoramic studies of field ionization in lithium [10]. Rydberg states were excited using the methods described earlier. A dc field was applied to exhibit the Stark structure. To show the onset of spontaneous field ionization, the high voltage pulse was delayed a few microseconds and a timing gate was used to reject signals which appeared prior to that delay. With this scheme, stable Rydberg atoms produced signals, but atoms which spontaneously ionized during the delay period did not. When the signals were plotted so as to produce a Stark structure map, the levels simply vanished at the critical field. An example is shown in fig. 14. The states are $|\, m \,| = 1$ levels of lithium in the vicinity of $n = 19$. The dotted line is the locus given by eq. (3.7). The agreement of experiment with the predicted value for the threshold field is striking and there seems no reason to doubt that the simple classical model is, in some sense, realistic. Nevertheless, as we shall see, serious difficulties remain.

It should be pointed out that one can do a far more rigorous classical analysis than the above. The two-dimensional Kepler problem in an applied field has been solved to yield values for the critical field at which the motion becomes unbound [11]. The results disagree markedly with those of our simple one-dimensional treatment, and so do the quantum mechanical results, which we now consider.

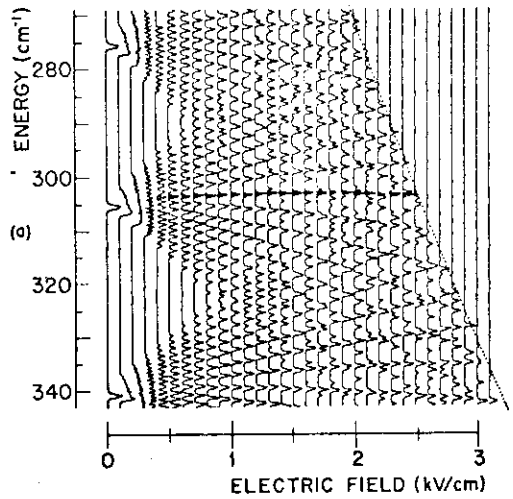

Fig. 14. Threshold ionization for $|m| = 1$ states of lithium in the vicinity of $n = 19$. Disappearance of the signal occurs when the ionization rate exceeds $3 \times 10^5\ \text{s}^{-1}$. The dotted line is the locus of stability given by eq. (3.17). (From ref. [10].)

3.2. Tunneling and field ionization

It is convenient to rewrite Schrödinger's equations for hydrogen in an applied field by letting $f_1(\xi) = \sqrt{\xi}\ f(\xi)$, $g_1(\eta) = \sqrt{\eta}\ g(\eta)$. Equations (2.23) become

$$f'' + \left(\frac{E}{2} + \frac{Z_1}{\xi} + \frac{1 - m^2}{4\xi^2} - \frac{F}{4}\xi\right) f = 0$$

$$g'' + \left(\frac{E}{2} + \frac{Z_2}{\eta} + \frac{1 - m^2}{4\eta^2} + \frac{F}{4}\eta\right) g = 0. \tag{3.8a, b}$$

If we let

$$(k_1(\xi))^2 = \frac{E}{2} + \frac{Z_1}{\xi} + \frac{1 - m^2}{4\xi^2} - \frac{F}{4}\xi, \tag{3.9a}$$

$$(k_2(\eta))^2 = \frac{E}{2} + \frac{Z_1}{\eta} + \frac{1 - m^2}{4\eta^2} + \frac{F}{4}\eta, \tag{3.9b}$$

then eqs. (3.8) become:

$$f'' + (k_1(\xi))^2 f = 0, \qquad g'' + (k_2(\eta))^2 g = 0. \tag{3.10a, b}$$

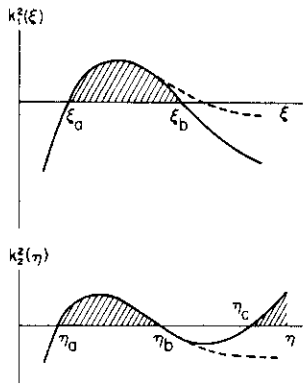

Fig. 15. Sketches of the effective energy function in an applied electric field for the parabolic functions $f_1(\xi)$ and $f_2(\eta)$. The allowed regions are shaded. The zero field values are shown dashed.

These equations describe one-dimensional motion with energy $k^2/2$. Figure 15 shows the behavior of k_1^2 and k_2^2. The allowed region is shaded. The ξ motion is confined to the region $\xi_a < \xi < \xi_b$; the η motion is allowed in the region $\eta_a < \eta < \eta_b$ and also $\eta > \eta_c$ where η_c is an outer turning point due to the field. It is evident that a system initially in the inner allowed region of η will eventually escape by tunneling through the forbidden region $\eta_b < \eta < \eta_c$.

For high quantum numbers, this problem naturally lends itself to a WKB treatment. Let us assume for the moment that the tunneling rate is low and that the energy of the system is known. The WKB solution for the ξ-motion is

$$\int_{\xi_a}^{\xi_b} k_1(\xi)\,\mathrm{d}\rho = \left(n_1 + \frac{1}{2}\right)\pi \tag{3.11}$$

where the integer n_1 has the same meaning as in eq. (2.27). Equation (3.11) can be treated as an eigenvalue problem for Z_1, whose solution consequently fixes the value $Z_2 = 1 - Z_1$. (For the case of nuclear charge Z, this relation becomes $Z_2 = Z - Z_1$.) Thus the k_1 solution also leads to a solution for k_2 which will satisfy

$$\int_{\eta_a}^{\eta_b} k_2(\eta)\,\mathrm{d}\eta = \left(n_2 + \frac{1}{2}\right)\pi, \tag{3.12}$$

provided that the energy is correct. The barrier penetration factor is

$$\exp\left(-2\int_{\eta_b}^{\eta_c} |k_2(\eta)|\,\mathrm{d}\eta\right) \tag{3.13}$$

and the ionization rate is

$$\Gamma = \exp\left(-2\int_{\eta_b}^{\eta_c} |k_2(\eta)|\,\mathrm{d}\eta\right) \Big/ \left(4\int_{\eta_a}^{\eta_b} \frac{\mathrm{d}\eta}{k_2(\eta)}\right). \tag{3.14}$$

The denominator is the classical period of a particle trapped in the potential well.

The complication in carrying out such a calculation is that in general the energy is not known a priori, so that eqs. (3.11) and (3.12) have to be treated as a pair of coupled eigenvalue equations. The separation parameter, energy and ionization rate must all be obtained by some self-consistent procedure. Rice and Good [12] solved this problem using a WKB technique, and a compilation of tunneling rates using their method has been prepared by Bailey et al. [13]. Some typical results for $n = 14$ are shown in fig. 16. The curves are labeled by the quantum numbers $(n, n_1, n_2, |m|)$. The most striking feature of these curves is their steepness: the ionization rate increases by almost 10^6 as the field increases by 20%. This rapid rise is suggestive of an abrupt threshold for the onset of ionization, but this idea must be treated with some caution.

The experimental points in fig. 16 were obtained by measuring the distribution in time for the appearance of a single ion after excitation of an atom in a strong electric field [14]. Sodium rather than hydrogen was used, but for $m = 2$ states the non-hydrogenic perturbations were found to be negligible. The slope of the experimental data agrees well with the calculation; the slight displacement in field is within the uncertainty in the absolute calibration of the field.

Damburg and Kolosov [15] obtained an analytical expression for the field ionization rate from an asymptotic treatment of eq. (3.8b). Solutions in the two allowed regions were asymptotically joined within the forbidden region. Joining the solutions required varying the energy about the bound state solution, that is, by introducing an energy width into the state; the lifetime was then obtained from the energy width. The result is

$$\Gamma = \frac{(4R)^{2n_2+m+1}}{n^3 n_2!\,(n_2+m)!} \times \exp\left[-\tfrac{2}{3}R - \tfrac{1}{4}n^3F\left(34n_2(n_2+m) + 46n_2 + 7m^2 + 23m + \tfrac{53}{3}\right)\right], \tag{3.15}$$

where $R = (-2E)^{3/2}/F$. E is the energy calculated through 4th order in

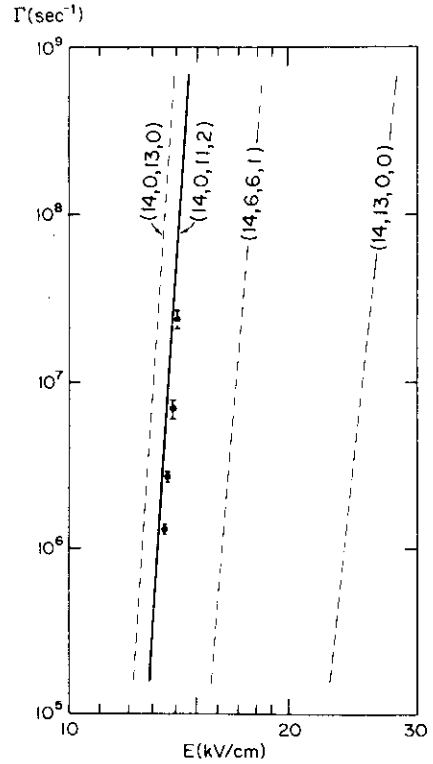

Fig. 16. Experimental ionization rates for a hydrogen-like state of sodium vs. applied electric field. The state is $n = 14$, $n_1 = 0$, $n_2 = 11$, $|m| = 2$. The dashed lines are the theoretical values of Rice and Good (ref. [12]); the solid line is interpolated from their results. (From ref. [14].)

the field F. The rates at low fields are in good agreement with results from numerical solutions to eqs. (3.8).

At high ionization rates, all approximation methods break down. The problem of calculating the complex energy of hydrogen in a strong field continues to attract wide attention, but rather than to discuss more elegant theoretical methods let us turn to some rather fundamental problems in understanding how real atoms ionize.

3.3. Discrepant views of field ionization

We have discussed field ionization from the simplest considerations of energy and from the elementary ideas of quantum mechanical tunneling.

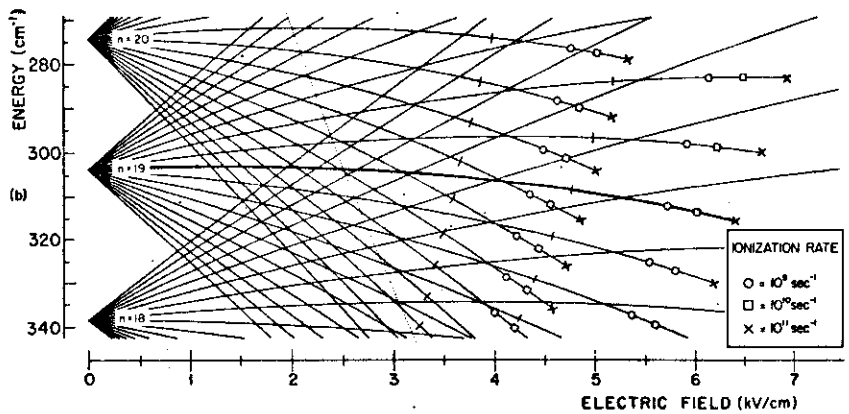

Fig. 17. "Classical" field ionization vs. tunneling for $n = 14$ levels of hydrogen. The field where the ionization rate due to tunneling equals the radiative decay rate is indicated by a dot. Level broadening due to ionization becomes conspicuous shortly above this value. The classical threshold field is indicated by the dashed line.

We have shown experimental data which supports each description and so it is natural to expect that the two descriptions are consistent, the classical being a limiting result of the quantum mechanical treatment. Matters, as it turns out, are more complicated.

Figure 17 shows several hydrogenic energy levels of the $n = 19$ manifold. Spontaneous field ionization shortens the life of each state and causes an energy broadening

$$E_i = \Gamma. \tag{3.16}$$

The level widths ΔE_i are shown; they increase so rapidly with field that the levels rather abruptly disappear. The classical threshold, eq. (3.7), is shown on the same plot. It has little to do with the disappearance of levels due to tunneling. Note, for instance, that tunneling causes the levels to ionize with increasing field in order of increasing energy, whereas the classical threshold predicts the reverse behavior. For the upper levels the threshold field and tunneling field differ by factors of greater than two!

3.4. Resolution of the discrepant views

The "saddlepoint" model provides a simple answer to the question "at what field is ionization energetically possible?" It has essentially nothing to say about the ionization rate, though the data in fig. 14, as well as a

great many other observations, show that the rate grows very rapidly at the threshold field. These observations are generally on alkali metals or other simple atoms; the fact that the atoms are not exactly hydrogenic is crucial.

Let us consider the broadening of a particular Stark level of hydrogen, A, as shown in fig. 18. Note that many levels from higher terms cross A, and that these levels may be extremely broad due to field ionization. Thus in the presence of an electric field, each Stark level is actually embedded in a "sea" of higher lying levels, both discrete and continuous.

The degenerate "sea" of levels has no effect on the dynamics of hydrogen because the states possess definite symmetry. This is a dynamical symmetry [16] inherent in the electric field problem with a Coulomb potential. The separability of Schrödinger's equation in parabolic coordinates is another consequence of the symmetry. The symmetry is only exact, however, for a pure Coulomb potential. Any perturbation to the potential, for instance the core interaction in an alkali metal atom, will upset the symmetry and cause the hydrogenic Stark levels to mix. One consequence of such a perturbation is the anti-crossing displayed by alkali atom Stark levels, as shown in fig. 8. A second consequence is the mixing of a stable state with a decaying state, causing the former also to decay. This is the underlying mechanism of field ionization for fields above the classical threshold value but below the value for which tunneling is important.

We can make these ideas quantitative by considering a simple example of a two level system. The energies, W_a and W_b, respectively depend on the field, and in the absence of any perturbation levels are degenerate at some value of the field, F_0. We shall assume that level a decays by ionization at rate Γ_a (which can also depend on the field), but that the

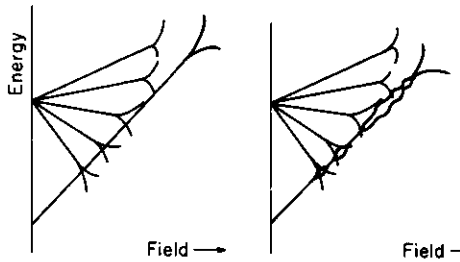

Fig. 18. Sketch of Stark levels of hydrogen in strong electric fields (left), and of an alkali metal atom (right). Hydrogenic Stark levels do not interact; in an alkali the levels can mix, causing an otherwise stable level to decay. The level widths indicate the decay rates.

decay rate of state b is negligible. The states are coupled by a perturbation, V.

If we treat the energies as complex quantities then the eigenvalue equation is

$$\begin{vmatrix} W_a - i\Gamma_a/2 - W & V \\ V^* & W_b - W \end{vmatrix} = 0. \tag{3.17}$$

For simplicity, consider the solution at the level crossing, where $W_a = W_b = W_0$, for the case $\Gamma_a \gg V$. The energies are, approximately

$$W_a' = W_0 - i\Gamma_a/2, \qquad W_b' = W_0 - 2i\,|\,V\,|^2/\Gamma_a. \tag{3.18}$$

The real parts of the energy are equal, showing a violation of the "no-crossing" theorem. Such behavior was first pointed out by Lamb [17]

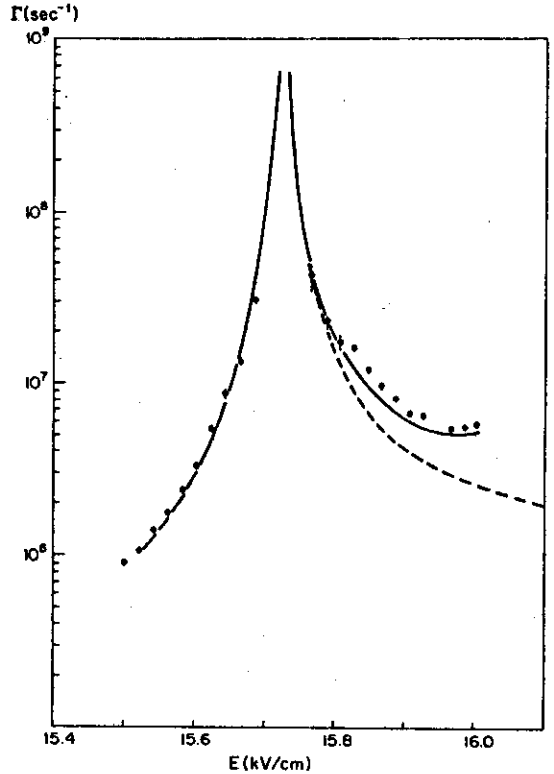

Fig. 19. Field ionization at a level crossing, as observed in sodium. Dots are experimental points, solid lines are calculated values. (From ref. [14].)

in his discussion of the effect of radiative damping on the fine structure of hydrogen. More importantly, state b has an imaginary part. The damping rate $\Gamma_b' = 4V^2/\Gamma_a$ is small compared to Γ_a, but in many experimental situations it can be significant.

The situation is, in general, more complicated than this model suggests due to the simultaneous interaction of many levels. Nevertheless, in one case where only a few levels are important, the analysis gives good agreement with observation, as shown in fig. 19.

There is a close analogy between field ionization in the "classical" region and autoionization in a multi-electron atom. In each case degenerate stable and continuum levels are coupled by a perturbation which mixes some of the continuum character into the stable state. If the perturbation is known the decay rate can be calculated.

The basic principle of field ionization appears to be well understood, but a general theory for calculating the ionization rates for one-electron atoms is lacking. Although major features of field ionization can often be predicted with confidence, many applications require a detailed understanding of the ionization rates, frequently for adjacent levels. In such cases there is at present no alternative to careful experimental observations. There is a clear need for new theoretical approaches.

4. Atoms in strong magnetic fields

4.1. Background

Magnetic fields have played a useful and occasionally very important role throughout the history of atomic physics. The Zeeman effect, for example, provided the first direct evidence of the electromagnetic origin of light, while the Stern–Gerlach experiment proved the reality of spatial quantization. Over the years, studies of atom–field interactions have provided important keys to understanding angular momentum coupling schemes and various spin-dependent interactions in atoms. The magnetic interaction in these studies was generally feeble, however, because the Zeeman effect is intrinsically tiny compared to the electrostatic interaction. There are two reasons for this. First, laboratory-size magnetic fields are small. The atomic unit of field is $e/a_0^2 = 1.7 \times 10^3$ T (1 tesla $= 10^4$ gauss), whereas useful laboratory fields are generally less than 30 T. Second, the coupling constant for atoms with the magnetic field, the Bohr magneton, μ_0 is also small ($\mu_0 = \alpha/2$ atomic units). In contrast,

electric dipole matrix elements tend to grow as n^2. Thus, even though the Zeeman effect is first order while the Stark effect is second order, the latter can be much larger due to the possibility of giant polarizability.

At very high magnetic fields, however, the diamagnetic interaction, which increases quadratically with field, is important. For highly excited atoms the diamagnetic susceptibility actually becomes gigantic, offering the opportunity of studying atomic structure experimentally under very strong field conditions. Part of the attractiveness of these experiments is that the problem has no general solution. In fact, our theoretical understanding is so poor even qualitative insight is lacking. It can be argued that the non-relativistic problem of hydrogen in a magnetic field of arbitrary strength is the principal remaining unsolved problem in the elementary quantum mechanics of a one-electron atom. In such a situation, one can expect that new experiments will lead to new theoretical insights. As we shall see, this is exactly the case.

4.2. The basic Hamiltonian

The interaction of a charged particle q with a magnetic field $\boldsymbol{B} = \nabla \times \boldsymbol{A}$, where $\boldsymbol{A}$ is the vector potential, is governed by the canonical momentum

$$\boldsymbol{p} = m\boldsymbol{v} + \frac{q}{c}\boldsymbol{A}, \tag{4.1}$$

so that the classical Hamiltonian is

$$H = \frac{1}{2m}\left(\boldsymbol{p} - \frac{q}{c}\boldsymbol{A}\right)^2. \tag{4.2}$$

If we consider an electron of charge $-e$ under the combined influence of an applied field and a central potential $V(r)$, then the Hamiltonian in atomic units is, neglecting electron spin

$$H = \tfrac{1}{2}(\boldsymbol{p} + \alpha\boldsymbol{A})^2 + V(r). \tag{4.3}$$

The most convenient gauge for treating a uniform field is the Coulomb gauge in which

$$\nabla \cdot \boldsymbol{A} = 0. \tag{4.4}$$

In this gauge, the Hamiltonian becomes

$$H = \frac{p^2}{2} + V(r) + \alpha\boldsymbol{p} \cdot \boldsymbol{A} + \tfrac{1}{2}\alpha^2 A^2. \tag{4.5}$$

For a uniform field along the z-axis $\boldsymbol{A} = (\boldsymbol{B} \times \boldsymbol{r})/2$, and we have

$$H = H_0 + \frac{\alpha}{2}\boldsymbol{L} \cdot \boldsymbol{B} + \frac{1}{8}\alpha^2 B^2 r^2 \sin^2\theta. \tag{4.6}$$

The first term is the Hamiltonian for the free atom, the second term is the orbital paramagnetic interaction and the last term is the diamagnetic interaction, H_d. Our major concern will be the structure in fields where the diamagnetic interaction plays a principle role, but for completeness we shall write the Hamiltonian with the major spin-dependent terms explicitly displayed:

$$H = H_0 + H_p + H_d + H_s + H_n, \tag{4.7}$$

where

$$H_p = \frac{\alpha}{2}(\boldsymbol{L} + g_e\boldsymbol{S}) \cdot \boldsymbol{B}, \qquad H_d = \frac{\alpha^2}{8}B^2 r^2 \sin^2\theta, \tag{4.8a, b}$$

$$H_s = \xi(r)\boldsymbol{L} \cdot \boldsymbol{S}, \qquad H_n = a(\boldsymbol{I} \cdot \boldsymbol{J}) + \frac{\alpha}{2}g_I'\boldsymbol{I} \cdot \boldsymbol{B}. \tag{4.8c, d}$$

g_e and g_I' are the electronic and nuclear g factors, respectively, while $\boldsymbol{S}$ and $\boldsymbol{I}$ are their respective spins. $\xi(r)$ is the radial spin orbit operator, and a is the hyperfine constant.

4.3. *Low field solution*

At low magnetic fields the spin orbit interaction couples $\boldsymbol{L}$ and $\boldsymbol{S}$ to form total electron angular momentum $\boldsymbol{J}$, and the hyperfine interaction couples $\boldsymbol{J}$ and $\boldsymbol{I}$ to form $\boldsymbol{F}$. As the field increases the electron-field interaction H_p exceeds the hyperfine interaction H_n and, at a much higher field, eventually exceeds the spin-orbit interaction H_s (Paschen–Back effect). The electronic energy is not significantly altered by any of these interactions, and analyzing their effects is chiefly a matter of properly recoupling the angular momentum [2]. Such problems have ben extensively studied, and since our goal is to understand high field behavior where these interactions are unimportant, let us simply neglect all effects of electronic and nuclear spin, and deal with a hypothetical hydrogen atom governed by the Hamiltonian

$$H = \frac{p^2}{2} - \frac{1}{r} + \frac{\alpha}{2}\boldsymbol{L} \cdot \boldsymbol{B} + \frac{1}{8}\alpha^2 B^2 r^2 \sin^2\theta. \tag{4.9}$$

If we neglect the last term and treat the third as a perturbation, we obtain

$$E(n, \ell, m) = -\frac{1}{2n^2} + \frac{\alpha}{2}mB. \tag{4.10}$$

ℓ remains a good quantum number, and each manifold (n, ℓ) is separated into $2\ell + 1$ sublevels split by the linear Zeeman energy $(\alpha/2)B$.

The diamagnetic interaction $H_d = \alpha^2 B^2 r^2 \sin^2\theta/8$ couples states with $\Delta\ell = 0, \pm 2$, and Δn unrestricted. The only good quantum numbers are m_ℓ and parity. The diagonal matrix element for $m = 0$ or $m = \pm 1$ is [20]

$$\langle n, \ell, m \mid H_d \mid n, \ell, m\rangle = \frac{\alpha^2 B^2}{8} n^2 \frac{\left[5n^2 + 1 - 3\ell(\ell+1)\right](\ell^2 + \ell - 1 + m^2)}{(2\ell+3)(2\ell-1)}. \tag{4.11}$$

If we consider the $4p$, $m = 1$, states of hydrogen, the diamagnetic and paramagnetic terms are equal at $B = 2 \times 10^7$ gauss, which sets the scale for what we might call "strong diamagnetism." (The H_β line ($n = 4 \to 2$) has actually been observed at 2×10^4 T in the spectrum from a white dwarf star [18].) 2×10^4 T cannot really be considered a strong field as far as $n = 4$ states are concerned, however, for the diamagnetic interaction remains small compared to the electronic interaction. For true strong field behavior, the diamagnetic energy must be comparable to the Coulomb energy.

At low fields n is an approximate quantum number because the n-mixing perturbations are second order. The off-diagonal elements of H_d mix all members of each term having the same parity and the same value of m_ℓ. For hydrogen, where all the states within a a term are degenerate, H_d can be diagonalized by some operator which transforms the spherical representation into what we shall call the magnetic representation. The situation is reminiscent of the transformation from the spherical to the parabolic representation, except that the properties of the latter are known (the transformation coefficients are Clebsch–Gordon coefficients [19]), whereas the properties of the former are not. Nevertheless, the transformation can be carried out numerically. The result of such a computation is shown in fig. 20, which shows the charge density for the $n = 8$, $m = 0$ "magnetic states". We can label the states within the manifold (n, m) by a quantum number d which has the values $|m|$, $|m + 1|, \ldots, (n - 1)$. Since parity is also a good quantum number, the submanifold is further split into two groups with d even or odd. The

diamagnetic energy for these states is sketched in fig. 21. If we write the diamagnetic energy as

$$\langle H_d \rangle = k(d)B^2 \tag{4.12}$$

then it can be seen that $k(d)$ has a maximum value for the state most spread out in the x–y plane, and a minimum value for the state localized to the z-axis. These are respectively labeled by $d = 0$ and $d = 7$ in fig. 20. Physically, the $d = 0$ state has the largest diamagnetic susceptibility in the $n = 8$ manifold since $\langle x^2 + y^2 \rangle$ is a maximum, whereas the $d = 7$ state has the smallest. The low ℓ states have the largest values of $\langle r^2 \rangle$. Consequently, they have the largest diamagnetic energy, so that they tend to be correlated with the low d states. Similarly, high ℓ states tend to be correlated with high d states. As we shall see, this correlation can play an important role in the appearance of diamagnetic spectra. Nevertheless, it must be kept in mind that ℓ is completely mixed by the diamagnetic interaction, and that each state is composed of all possible value of ℓ having the same parity and same value of m_ℓ.

4.3.1. Solution at slightly higher field

As the magnetic field is increased, $\langle H_d \rangle$ starts to become significant compared to the term separation. When this occurs, matrix elements of H_d which are off-diagonal in n become important. Again, lacking an analytical solution for the eigenstates and energies, we can resort to numerical computation by expanding the basis set to include adjacent terms with the same parity and m_ℓ. The result for one such computation is shown in fig. 22. (The states are even parity, $m = 0$). When the terms overlap the levels appear to repel strongly, and the regularities are lost.

Somewhat unexpectedly, the picture looks simple at higher values of n. Figure 23 shows the level structure in the vicinity of $n = 28$ for even parity, $m = 1$ states. The diamagnetic interaction appears to be essentially linear in B^2 even where the terms overlap. The experimental spectra overlayed on the plot are of Na [21]. The excitation was a p–d transition so that the intensity of each level is proportional to the amount of d state in the level. For the reasons explained above, the intensity is strongest for the highest level.

4.4. Very high field solution

In very high magnetic fields it is natural to regard the Coulomb interaction as a perturbation and take the free electron problem as the starting

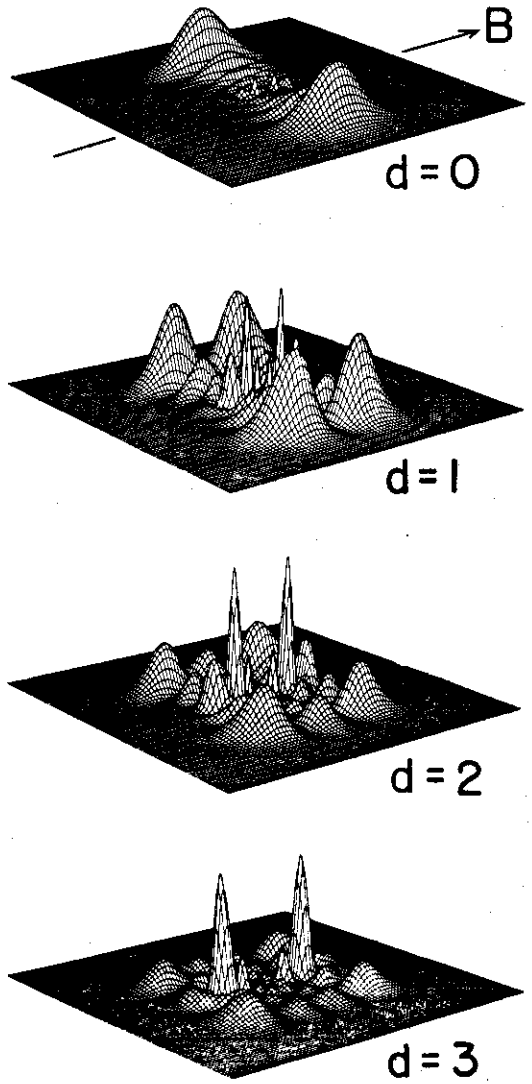

Fig. 20. Plots of charge density for $n = 8$, $|m| = 0$ states of hydrogen in a magnetic field, drawn as in fig. 1. The index d serves to label the states but it is not the eigenvalue of any known operator.

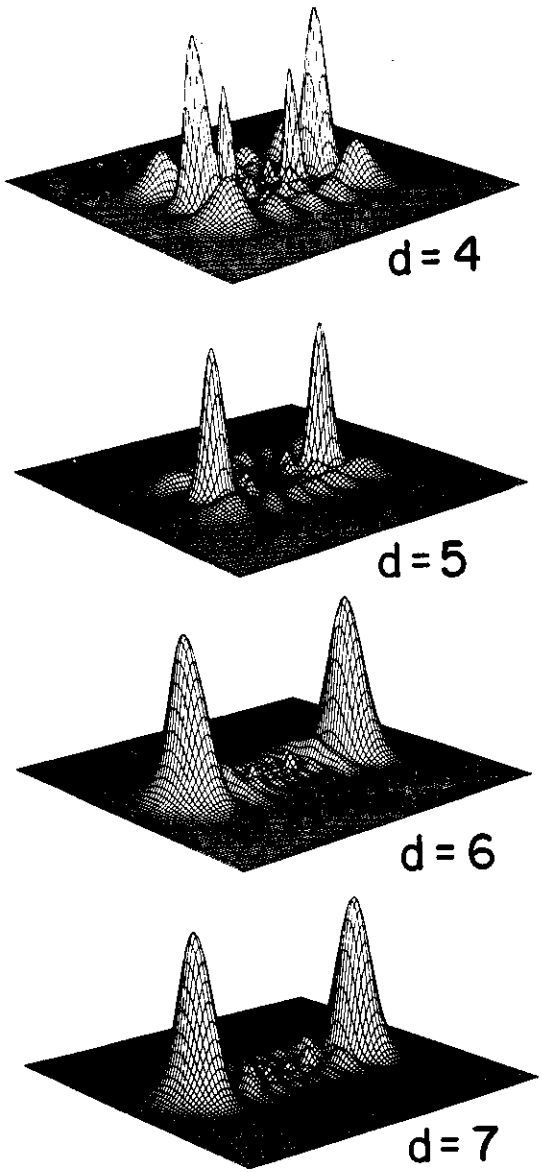

Fig. 20 continued.

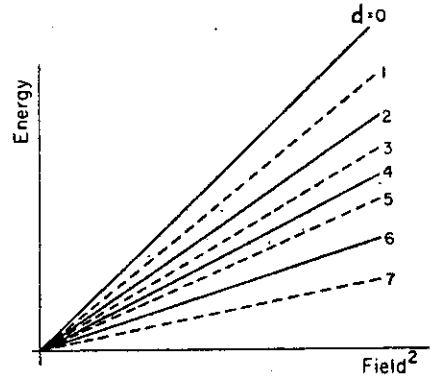

Fig. 21. Sketch of the diamagnetic energy vs. the square of the magnetic field for $n = 8$, $m = 0$ levels of hydrogen. Even parity levels are solid; odd parity levels are dashed.

point. The theory for a free electron in a magnetic field was initially worked out by Landau, and the details are available in many quantum mechanics texts. The Hamiltonian is

$$H_0 = \tfrac{1}{2}(\boldsymbol{p} + \alpha \boldsymbol{A})^2. \tag{4.13}$$

For a uniform field along the z axis the energy can be written

$$E = E_z + E_n \tag{4.14}$$

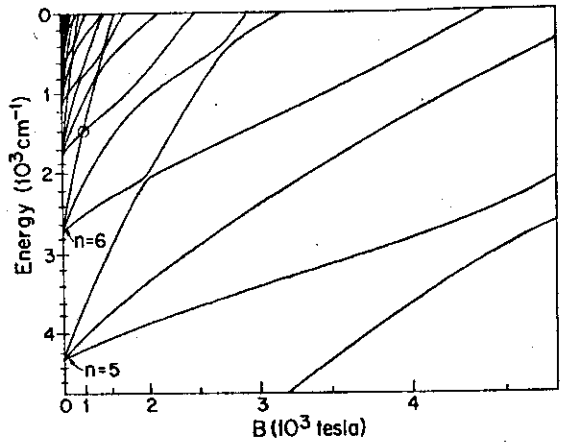

Fig. 22. Energy levels of even parity $|m| = 0$ states of hydrogen in the vicinity of $n = 6$, plotted on a scale quadratic in B. Note the strong repulsions between many levels. (From ref. [25].)

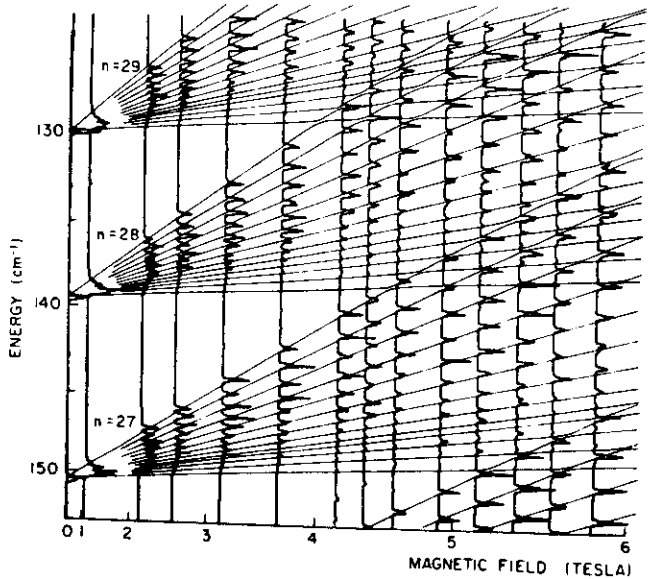

Fig. 23. Calculated and observed diamagnetic structure of even parity $|m|=2$ states of sodium vs. field (plotted on a squared scale). (From ref. [21].)

where

$$E_n = \left(n_c + \tfrac{1}{2}\right)\hbar\omega_c = \left(n_c + \tfrac{1}{2}\right)\alpha B; \tag{4.15}$$

n_c is an integer and ω_c is the cyclotron frequency eB/mc ($= \alpha B$ atomic units). $E_z = k^2/2$ is the energy of free motion along the field. The propagation vector k is unrestricted.

The wave function is, in cylindrical coordinates,

$$\psi(\eta, m, k) = NS_{n,m}(\rho)e^{im\phi}e^{ikz}, \tag{4.16}$$

where m is the magnetic quantum number, N is for normalization, and

$$S_{n,m}(\rho) = \rho^{|m|}e^{-\rho^2/4R^2}L_{n+|m|}^{|m|}(\rho^2/2R^2); \tag{4.17}$$

$R = (eB/hc)^{-1/2} = (\alpha B)^{-1/2}$ is the cyclotron radius, $n_c = n + (m + |m|)/2$.

If we attempt to treat the Coulomb interaction as a perturbation by writing

$$H = H_0 - \frac{1}{r}, \tag{4.18}$$

we are immediately faced with the problem that the magnetic interaction vanishes along the field whereas the Coulomb interaction does not, so that a perturbative treatment is fundamentally inadequate. To make matters worse, the Hamiltonian eq. (4.18),

$$H = \frac{p^2}{2} + \frac{\alpha}{2}\boldsymbol{L}\cdot\boldsymbol{B} + \frac{1}{8}\alpha^2B^2\rho^2 - \frac{1}{\sqrt{\rho^2+z^2}}, \tag{4.19}$$

is inseparable and we lack any sort of general solution.

One promising approach to the problem is the so-called adiabatic approximation [22] which rests on the assumption that frequency of the transverse motion is high compared to the frequency of longitudinal motion. The z motion takes place in an effective potential which is evaluated by averaging the longitudinal Coulomb interaction over many cycles of the cyclotron frequency. The method works well for states which have low longitudinal momentum, that is, states which are localized in the x–y plane, but it has not yet been extended to states of arbitrary z-momentum.

4.5. *The quasi-Landau resonances*

In 1969 Garton and Tomkins [23] discovered a periodic modulation in the absorption spectrum of barium in a field of 2.5 T. The modulation extended well above the zero field ionization limit of the atom and had a period of close to $1.5\omega_c$ at the limit, (ω_c is the cyclotron frequency). At higher energy the period approached ω_c, as one might expect for a free electron. The modulation was successfully explained by Edmonds [24] and Starace [22] using a semiclassical approach. Their analysis shows both the power and the limitations of the adiabatic approximation.

An important clue to the nature of the quasi-Landau resonances is that they are observed in the σ spectrum ($\Delta m_\ell = \pm 1$) but not in the π spectrum ($\Delta m_\ell = 0$). The σ lines arise from states which tend to be localized in the x–y plane, whereas the π line comes from a state with a node in the x–y plane. Edmonds and Starace argued that a reasonable approximation for the σ states is to neglect the z motion and treat the problem as two dimensional. The effective potential is

$$V(\rho) = -\frac{1}{\rho} + \frac{m^2 - \frac{1}{4}}{2\rho^2} + \frac{\alpha}{2}mB + \frac{1}{8}\alpha^2B^2\rho^2. \tag{4.20}$$

The energy levels can then be found from a WKB argument

$$\int_{\rho_1}^{\rho_2}(2E - 2V(\rho))^{1/2}\,\mathrm{d}\rho = \left(n + \frac{1}{2}\right)\pi, \tag{4.21}$$

where ρ_1 and ρ_2 are the inner and outer turning points, respectively. The separation between levels can be found by evaluating

$$\frac{\mathrm{d}E}{\mathrm{d}n} = \frac{\pi}{\int_{\rho_1}^{\rho_2}\left[2E - 2V(\rho)\right]^{1/2}\mathrm{d}\rho}. \tag{4.22}$$

At $E = 0$ the result is $\mathrm{d}E/\mathrm{d}n = 1.5\ \omega_c$. Numerical evaluation for other energies shows that the spacing slowly decreases as the energy becomes higher.

The quasi-Landau resonances have attracted wide attention because they demonstrate dramatically that motion in the strong mixing region (the region where electric and magnetic forces are comparable) can be understood by simple dynamical arguments. Nonetheless, the WKB explanation is by no means complete. It cannot be used to predict line intensities and it fails to show how the states relate to low field states. More seriously, it deals with only a small subset of the possible states and fails to deal with the general problem of atomic structure in a strong magnetic field. Fortunately, a combination of recent experimental and computational advances suggest that the general problem may be more tractable than anyone thought.

4.6. Intermediate field behavior

One reason for the prominence of the quasi-Landau resonances in absorption spectra is that Stark-mixing of levels due to the motional electric field tends to average together nearby lines, thereby revealing general patterns in line strength. Nonetheless, the resonance can still be observed in fully resolved spectra. Figure 24, for instance, shows spectra for even parity $m_\ell = -2$ states of sodium. Lines have been drawn through the uppermost level of each manifold starting at low field. These levels evolve into the quasi-Landau resonances. In fig. 25 a single sweep is displayed magnified; the dominant levels show an energy separation approaching 1.5 ω_c at $E = 0$. Under conditions of low resolution the spectrum would show smooth periodic fluctuations, the signature of quasi-Landau resonance.

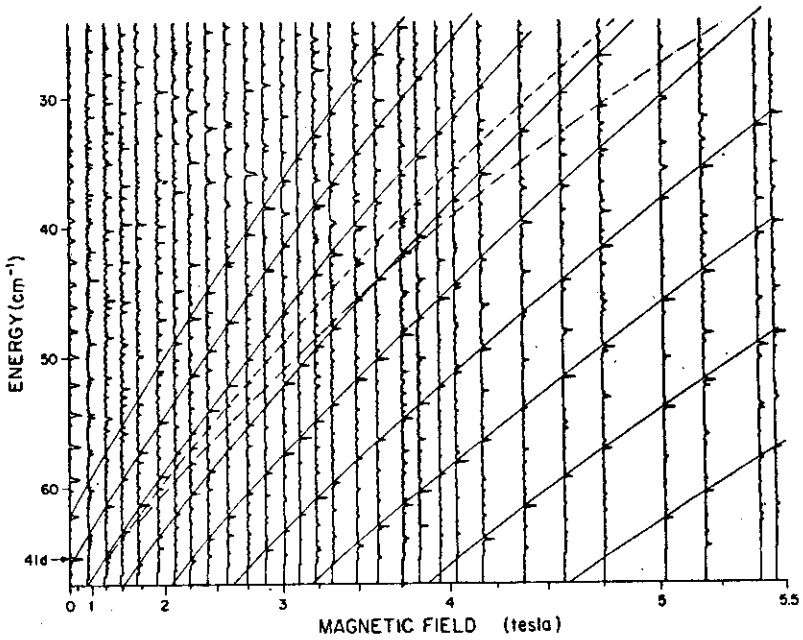

Fig. 24. Experimental excitation curves for even parity, $m_\ell = -2$ states of sodium vs. field (plotted on a squared scale). Solid lines indicate the evolution of the highest level for several n manifolds. The dashed and dash–dot lines show the second and third highest levels of the $n = 40$ manifold, respectively. The evolution is most clearly seen by sighting along the drawn lines.

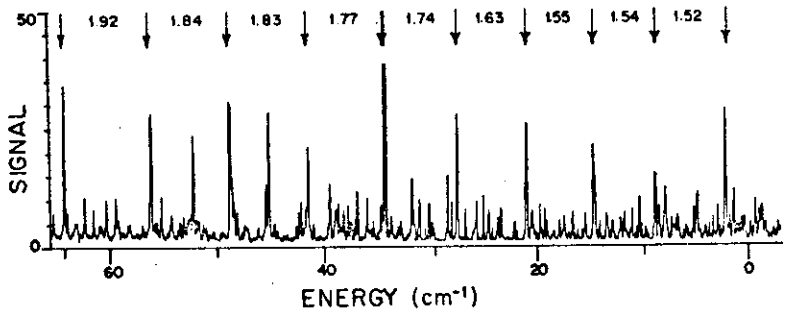

Fig. 25. Quasi-Landau spectrum, taken from data in fig. 24. The arrows indicate the quasi-Landau levels. The numbers between the arrows give the level separation in units of $\hbar\omega_c$. The spacing increases with binding energy from the value of 1.5 at $E = 0$, in agreement with a WKB analysis. (From ref. [26].)

Close inspection of fig. 24 shows how the quasi-Landau resonances originate. They arise by a transfer of oscillator strength from among all of the levels in each n-manifold to the highest level of the manifold. The transfer is not complete, however, for the second highest level is also visible (dashed line). Other intermediate levels are also visible, but at low intensity.

In fig. 26 we show even parity $m_\ell = -1$ states of sodium. These states have a node in the x–y plane, and are not expected to show the quasi-Landau resonances. Instead, we observe a multitude of lines of approximately equal intensity. Under low resolution conditions the spectrum would be featureless, but under high resolution some rather startling facts emerge. The first unexpected observation is that the levels evolve smoothly with no apparent level repulsions. Thus each state preserves its low field character into the strong mixing regime, exactly as in the case of the Stark structure of hydrogen. The second unexpected feature is that corresponding members of each manifold (highest, second

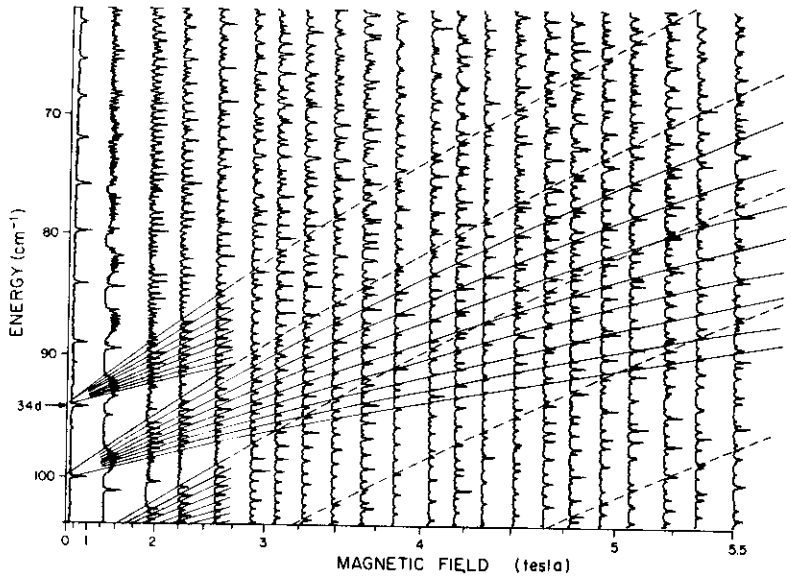

Fig. 26. Same as fig. 24, except that the states are even parity $m_\ell = -1$, and the energy range is displaced. The dashed lines are drawn to indicate the evolution of the highest level for several n manifolds. Note that the corresponding levels of adjacent n manifolds are equally spaced. The levels are most conspicuous when viewed close to the plane of drawing, along the dashed lines.

highest, etc.) all show the *same* periodicity. Thus the quasi-Landau structure appears to be a general property of *all* states of the atom, not merely those localized in the x–y plane. Structure in the strong mixing regime appears to be characterized by simple regularities, a rather unexpected finding in view of the theoretical complexity of the problem.

4.7. The possibility for a complete solution

There is something of a paradox in the data of fig. 26: the levels appear to cross each other in defiance of the "no-crossing" theorem. There are two possible explanations. Either the levels actually repel, but at a scale too small to see, or there is some hidden symmetry in the problem, analogous to the dynamic symmetry of the Stark problem, which allows degeneracies to occur freely. As we shall see, the true explanation probably combines both of these possibilities.

We have investigated level-crossing behavior by numerically diagonalizing the Hamiltonian using procedures similar to those of the Stark problem. Results for some low-lying terms have already been shown, fig. 22. Most of the levels repel as expected, though there are some apparent crossings. (One apparent crossing is encircled.) More careful studies of these crossings show that they are actually weak anti-crossings [26]. At high values of n, as in fig. 27, there are no conspicuous anticrossings. The levels display the simple non-interactive structure we observed in the data

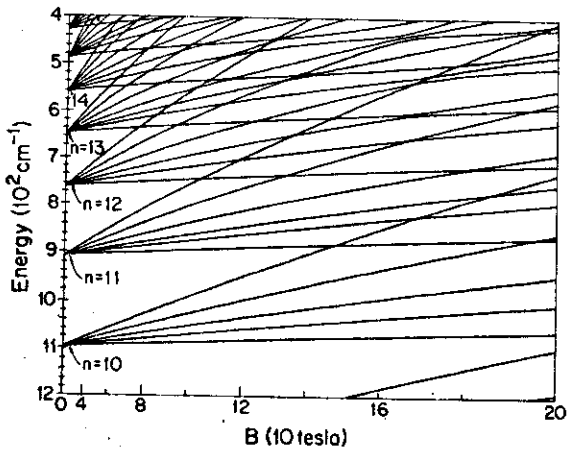

Fig. 27. Energy of hydrogen as a function of magnetic field (plotted on a squared scale) for terms in the range $n = 10-14$. (From ref. [25].)

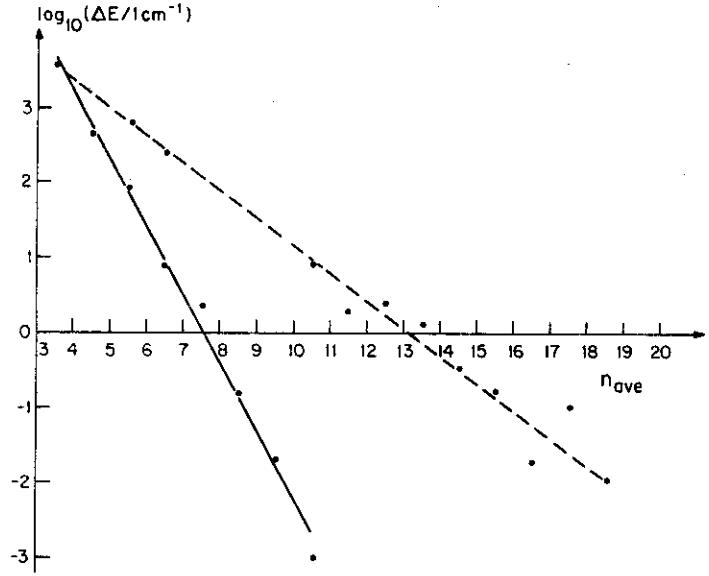

Fig. 28. Calculated anti-crossing separation as a function of $\bar{n}$, the geometric mean of the principal quantum number of adjacent manifolds. Solid line: lowest energy state of $n + 1$ and highest state of n. Dashed line: lowest energy state of $n + 1$ and the "middle" energy state of n. (From ref. [25].)

of fig. 26. Of course, such diagrams cannot be used to determine whether or not levels cross, for numerical computations have finite resolution. Nevertheless, if we study how the level repulsions vary with n, we find a striking decrease: the separations decrease exponentially with n, or even faster! Figure 28 shows the n-dependence of some calculated level repulsions. What we can conclude is that although the levels may never truly cross, the repulsions become so small that they effectively cross. Thus, if one writes the Hamiltonian as $H = H_0 + V$, where H_0 contains some symmetry which allows the levels to cross, and V mixes the eigenstates of H_0 and causes the levels to anti-cross, V has such a small effect at high n that it can be safely neglected. (For example, the effect of V will be small compared to the width of levels due to spontaneous radiation, which decreases only as n^{-3}.) This identification is a tantalizing prospect, for H_0, which is inherently separable, should have an exact solution. For the present, the problem is unsolved. Nevertheless, our "existence proof", if one can so dignify arguments based essentially on numerical computation, gives hope that the last elementary problem in

the quantum mechanics of the one-electron atom may be nearing a solution.

Much of the research reported here was carried out by students and former students working with me at M.I.T. Major contributions were made by Michael G. Littman, Myron L. Zimmerman, Michael M. Kash and Jarbas C. Castro. William P. Spencer generated the charge density plots of Rydberg atoms. Michael Kash was most helpful in preparation of this manuscript. The work at M.I.T. was funded by the National Science Foundation, the Joint Services Electronics Program and the Department of Energy.

References

[1] A. Khadjavi, A. Lurio and W. Happer, Phys. Rev. 67 (1968) 128.
[2] I. I. Sobelman, An Introduction to Atomic Spectra (Pergamon Press, Oxford, 1972).
[3] C. Fabre and S. Haroche, Opt. Comm. 15 (1975) 254.
[4] H. A. Bethe and E. E. Salpeter, Quantum Mechanics of One- and Two-Electron Atoms (Springer-Verlag, Berlin, 1957).
[5] H. J. Silverstone, Phys. Rev. A18 (1978) 1853.
[6] P. M. Koch, Phys. Rev. Lett. 41 (1978) 99.
[7] H. J. Silverstone and P. M. Koch, J. Phys. B12 (1979) L537.
[8] M. L. Zimmerman, M. G. Littman, M. M. Kash and D. Kleppner, Phys. Rev. A20 (1979) 2251.
[9] W. Cooke and T. Gallagher, Phys. Rev. A17 (1978) 1226.
[10] M. G. Littman, M. M. Kash and D. Kleppner, Phys. Rev. Lett. 41 (1978) 103.
[11] D. Banks and J. G. Leopold, J. Phys. B9 (1977) 1.
[12] M. H. Rice and R. H. Good, Jr., J. Opt. Soc. Am. 52 (1962) 239.
[13] D. S. Bailey, J. R. Hiskes and A. C. Riviere, Nucl. Fus. 5 (1965) 41.
[14] M. G. Littman, M. L. Zimmerman and D. Kleppner, Phys. Rev. Lett. 37 (1976) 486.
[15] R. J. Damburg and V. V. Kolosov, J. Phys. B12 (1979) 2637.
[16] K. Helfrich, Theor. Chim. Atom 24 (1972) 271.
[17] W. E. Lamb, Phys. Rev. 85 (1952) 259.
[18] J. R. D. Angel, Astro. J. 216 (1977) 1.
[19] D. Park, Z. Phys. 159 (1960) 155.
[20] L. I. Schiff and H. Snyder, Phys. Rev. 55 (1939) 59.
[21] M. L. Zimmerman, J. C. Castro and D. Kleppner, Phys. Rev. Lett. 40 (1978) 1083.
[22] A. F. Starace, J. Phys. B6 (1973) 585.
[23] W. R. S. Garton and F. S. Tomkins, Astrophys. J. 158 (1969) 839.
[24] A. R. Edmonds, J. Phys. Paris Colloq. 31 (1970) C4.
[25] M. L. Zimmerman, M. M. Kash and D. Kleppner, Phys. Rev. Lett. 45 (1980) 1092.
[26] J. C. Castro, M. L. Zimmerman, R. C. Hulet, D. Kleppner and R. R. Freeman, Phys. Rev. Lett. 45 (1980) 1780.